EMU Notes in Mineralogy, Vol. 17 (2016), Chapter 6, 113–164

Iron minerals as archives of Earth's redox and biogeochemical evolution

CAROLINE L. PEACOCK[1], STEFAN V. LALONDE[2] and KURT O. KONHAUSER[3]

[1] *University of Leeds, School of Earth and Environment, Leeds, LS2 9JT, UK, e-mail: C.L.Peacock@leeds.ac.uk*
[2] *European Institute for Marine Studies, CNRS-UMR6538 Laboratoire Domaines Océaniques UMR 6538, Brest, France, e-mail: Stefan.Lalonde@univ-brest.fr*
[3] *University of Alberta, Department of Earth and Atmospheric Sciences, Edmonton T6G 2E3 Canada, e-mail: KurtK@ualberta.ca*

Abstract

Iron minerals provide sedimentary repositories of chemical information pertaining to Earth's redox and biogeochemical evolution, from before the Great Oxidation Event some 2.5 billion years ago, to more recent events occurring up to and into the Cenozoic Era. The most powerful chemical information recorded in iron minerals comes in the form of trace-element signatures, most notably their concentrations and stable isotope compositions. Here we provide an introduction to iron mineralogy and the processes responsible for the accumulation and preservation of trace-element signatures in iron minerals, focusing on the deposition of iron minerals in three key ancient sedimentary archives: banded iron formations, ferromanganese crusts and black shales. We introduce the theory and practical use of non-traditional trace-element stable-isotope systems in redox and biogeochemical research, focusing on the recent use of iron, molybdenum and chromium stable isotopes to shed light on the redox and biogeochemical information stored in iron-rich sediments. By analysing both trace-element concentrations and stable-isotope compositions recorded in iron minerals, iron-rich sedimentary archives are providing a unique window into the past, where changes in trace-element signatures shed light on major transitions in Earth's redox and biogeochemical evolution.

Introduction

This chapter provides a review of the use of iron minerals as repositories of chemical information pertaining to Earth's redox and biogeochemical evolution, from before the Great Oxidation Event some 2.5 billion years ago, to more recent events occurring up to and into the Cenozoic Era. The most powerful chemical information recorded in iron minerals comes in the form of trace element signatures, most notably their concentrations and stable isotope compositions. We begin our review by providing an introduction to iron mineralogy and the processes responsible for the accumulation and preservation of trace element signatures in iron minerals, focusing on the deposition of these minerals in three key ancient sedimentary archives: banded iron

DOI: 10.1180/EMU-notes.17.14

formations (BIF), ferromanganese crusts and black shales. We then review the theory and practical use of non-traditional trace element stable isotope geochemistry, and in particular the use of emerging non-traditional stable isotope systems, in palaeo redox and biogeochemical research. Finally we focus on how different trace element signatures, recorded in those ancient sedimentary archives, have helped provide a window into the past, where changes in trace element signatures can be interpreted to reflect transitions in Earth's redox and biogeochemical evolution.

1. Iron minerals as archives of chemical information

Iron (Fe) minerals exist over a very wide range of redox conditions. They are extremely efficient scavengers of other elements, and effectively archive chemical information about the fluids from which they form. In the marine realm, Fe minerals form chemical sediments and cements under a variety of aqueous conditions and geological settings; these range from rapid water-column precipitation in Fe-rich hydrothermal plumes upon mixing with bulk seawater to the slow formation of concretions and cements at redox boundaries in sediments, nodules, and hydrothermal chimneys. The ubiquity of Fe oxyhydroxides in the marine environment, both modern and ancient, and the fact that their composition is intimately linked to the chemistry of the waters from which they precipitate, make them especially promising recorders of the geochemical history of their formation waters. Specifically, the elemental and isotopic enrichments recorded in Fe minerals provide information on the redox state of the contemporaneous environment and the biogeochemical cycling of bio-essential metals, both of which are linked to primary productivity, carbon cycling, and ultimately the evolution of Earth's surface environments through time.

1.1. Iron mineralogy as a function of redox

Iron is the fourth most abundant element in the Earth's crust, where it exists predominantly as ferrous iron, Fe(II), in Fe-bearing silicate minerals (*e.g.* pyroxenes, amphiboles). As these minerals are weathered, Fe(II) is released into solution, largely oxidized to ferric iron, Fe(III), and then delivered to the oceans. Transport involves a continuum of different size fractions, defined as aqueous (<0.02 μm, mainly organically-bound Fe), nanoparticulate (0.02 to 1 μm, mainly Fe(III) oxyhydroxide minerals that are also closely associated with organic species), and larger particles (>1 μm); for further explanation of Fe size fractions see Raiswell and Canfield (2012). There is a myriad of different processes delivering Fe to the oceans, and the relative magnitudes of the associated Fe fluxes vary both spatially and temporally (recently reviewed by Boyd and Ellwood, 2010 and Raiswell and Canfield, 2012). In order of importance, processes supplying Fe to the global ocean include deposition of windborne dust (*e.g.* Jickells *et al.*, 2005), melting of glaciers and icebergs (*e.g.* Raiswell *et al.*, 2008), remobilization of Fe from submarine shallow-shelf systems (*e.g.* Poulton and Raiswell, 2002), Fe transport via rivers (*e.g.* MacKenzie *et al.*, 1979), and submarine hydrothermal emissions (*e.g.* Tagliabue *et al.*, 2010; Table 1). A significant

Table 1. Fe sources and estimated fluxes to the global ocean, compiled and discussed extensively by Raiswell and Canfield (2012).

Fe sources to the global ocean	Fe flux (Tg/yr)
Aeolian	1.53–3.03
Icebergs	0.9–1.38
Sediment Recycling	0.05–0.25
Riverine	0.14
Hydrothermal	0.05
Total	2.62–4.8

proportion of the riverine Fe flux is probably removed *via* biogeochemical processes in estuaries, while the remainder is deposited on the continental shelf (*e.g.* Boyle *et al.*, 1977; Boyd and Ellwood, 2010).

Once Fe reaches the oceans, and depending on prevailing geochemical conditions, it can be (re)precipitated *via* a number of different mechanisms as a variety of hydrogeneous and typically nanoparticulate Fe(II/III) minerals (for a review see Raiswell and Canfield, 2012). Because Fe is redox active, these minerals can form under almost all water column redox conditions. In addition, many of these minerals have considerable surface area with an amphoteric surface charge (*i.e.* can be either positively- or negatively-charged depending on aqueous pH), meaning that they are highly reactive towards both dissolved cations and anions. As such, hydrogeneous Fe minerals make ideal sedimentary archives of trace element concentrations and stable isotope compositions in contemporaneous seawater, recording elemental signatures over a wide range of redox regimes.

Under fully oxic water column conditions, when the concentration of dissolved O_2 is greater than ~10^{-6} molar, Fe(II) is oxidized to Fe(III), which precipitates primarily as the nanoparticulate and poorly crystalline Fe(III) oxyhydroxide, ferrihydrite [$Fe^{3+}_{4-5}(OH,O)_{12}$]. Ferrihydrite is metastable and ages to the more crystalline minerals goethite [α-FeOOH] or hematite [Fe_2O_3] (Cornell and Schwertmann, 2003). Under anoxic conditions, when the concentration of dissolved O_2 is below ~10^{-6} molar, a variety of different Fe(II/III) minerals are formed. In non-sulfidic anoxic conditions (total dissolved sulfide < 10^{-6} molar) a variety of non-sulfidized Fe minerals can precipitate, including ferrihydrite and/or ferrous carbonates (*e.g.* siderite [$FeCO_3$]) and ferrous phosphates (*e.g.* vivianite [$Fe_3(PO_4)_2{\cdot}8H_2O$]). In addition, a mixed Fe(II/III) layered double hydroxide can form, termed green rust (general formula $[Fe^{II}_{(1-x)}Fe^{III}_x(OH)_2]^{x+}{\cdot}[(x/n)A^{n-}{\cdot}\ (m/n)H_2O]^{x-}$ where $A^{n-} = CO_3^{2-}$, SO_4^{2-}, Cl^-, OH^-). While relatively rare today, recent research suggests that green rust might be an important reactive Fe phase in anoxic water columns that are devoid of free sulfide and rich in dissolved Fe(II) (termed ferruginous) (*e.g.* Zegeye *et al.*, 2012). Under sulfidic

anoxic conditions where free sulfide is present (total dissolved sulfide $\geqslant 10^{-6}$ molar; termed euxinic) reactive Fe is precipitated as Fe sulfides, first as metastable makinawite (FeS), which then ages to pyrite (FeS_2). The classification of oxic and anoxic environments, in terms of dissolved O_2 and sulfide, is taken from Berner (1981) who provides an extended discussion of Fe (and other) minerals that are thermodynamically stable in these geochemical regimes.

In ocean sediments Fe(II/III) minerals are subject to diagenesis, during which they can be reductively dissolved and reprecipitated. Reductive dissolution proceeds *via* two competing pathways (*e.g.* Canfield *et al.*, 1993a,b; Van Cappellen and Wang, 1996; Raiswell and Canfield, 1998; Haese, 2000), the first involving microbial reduction (dissimilatory Fe reduction, DIR) and the second involving abiotic reduction by dissolved sulfide, which diffuses upwards through the sediment column from a deeper zone of microbial sulfate reduction (*e.g.* Berner, 1964; Staubwasser *et al.*, 2006). If Fe(III) oxyhydroxides are reduced by DIR, reactive Fe can go through a repeated cycle of reductive dissolution, upward diffusion, oxidation and reprecipitation as Fe(III) oxyhydroxides or, with partial oxidation, reprecipitation as a myriad of other Fe(II/III) minerals as described above (*e.g.* Canfield, 1989; Staubwasser *et al.*, 2006). Ultimately, reduction of Fe(III) oxyhydroxides by dissolved sulfide removes Fe from the diagenetic cycle (*e.g.* Raiswell and Canfield, 1998). The diagenetic formation of Fe sulfide minerals constitutes a major sulfur and Fe exit channel that occurs at anoxic depths in the sedimentary pile where both reduction of Fe(III) and sulfate occur.

Use of Fe-rich sediments as archives of palaeo-seawater composition assumes that the Fe minerals provide a faithful record of seawater trace element concentrations and/or stable isotope compositions, despite their diagenetic history. In some sedimentary systems, where Fe(III) concentrations exceed organic carbon, Fe(III) oxyhydroxides can be preserved in the sediments without reductive dissolution (*e.g.* Konhauser *et al.*, 2005). Under different scenarios, where reductive dissolution is likely to have occurred, it is important to demonstrate that the diagenetic processes have not significantly effected the original trace element concentrations and/or stable isotope compositions at the bulk scale, *i.e.* that there has been minimal loss of Fe and elements of interest from the bulk archive over time, and minimal redistribution of the isotopes between the bulk archive and sedimentary pore-waters (*e.g.* Poulton and Canfield, 2006; Frierdich *et al.*, 2011; Robbins *et al.*, 2015). Indeed, in the case of some geochemical proxies, the environmental signal recorded by Fe minerals may be largely a diagenetic one (*e.g.* the case of Fe isotope compositions; section 2.4.1).

1.2. Uptake of trace elements by iron minerals

1.2.1. Iron oxyhydroxides

Iron oxyhydroxides are highly effective sorbents, a property born out of the functional group and electrostatic charging characteristics of their surfaces. Some minerals (*e.g.* clays) possess permanent surface charge as the result of structural defects or isomorphous substitution. Others, including most hydrated oxyhydroxide minerals (whether they be Fe oxyhydroxides, silicon oxides, titanium oxides, *etc.*), develop

surface charge as the result of pH-dependent surface functional group protonation/deprotonation reactions. These minerals develop a positive surface charge at low pH as surface sites are neutralized or rendered positively charged with the surface sorption of protons and a negative charge at high pH as progressive deprotonation occurs (*i.e.* they are amphoteric). Adopting a 1pK formalism for the representation of surface sites, then surface sites of Fe oxyhydroxides (including hydrous ferric oxide, HFO, which is synonymous with ferrihydrite) develop charge through the following protonation/deprotonation reaction:

$$>FeOH^{-0.5} + H^{+} \leftrightarrow >FeOH_2^{+0.5} \qquad pK_a = \sim 8 \tag{1}$$

where >FeOH denotes surface Fe hydroxyl functional groups (log acidity (pK_a) value for ferrihydrite given as an example and taken from *e.g.* Davis and Leckie (1978)). At pH values above and below ~8, surface sites, and thus the net charge on the mineral surface, will be predominately negatively or positively charged as $>FeOH^{-0.5}$ or $>FeOH_2^{+0.5}$, respectively. At pH ~8, surface sites of opposite charge are present in equal amounts and this is deemed the point of zero charge (PZC). Crucially, ferrihydrite, and other pure Fe oxyhydroxide surfaces in general, are characterized by PZC values around 8, and thus possess abundant negatively and positively charged sites that are strongly reactive under many natural conditions (*e.g.* Sverjensky and Sahai, 1996). Considering their ubiquity and propensity to form nanometre-scale aggregates with large surface areas (in some cases upwards of 600 m^2 per dry gram, Roden *et al.*, 2003), Fe oxyhydroxides provide the most prevalent positively charged reactive mineral surface found in nature (Cornell and Schwertmann, 2003). In contrast, the surfaces of silicate minerals generally possess PZC values around 2 (*e.g.* Ihler, 1979), and are thus strongly negatively charged under most natural conditions.

The surface chemistry of Fe oxyhydroxides has long been studied in relation to the sorption of contaminants in natural waters. Equilibrium surface complexation models (SCM), employing experimentally- and/or theoretically-derived parameters (*e.g.* stability constants for (de)protonation of the surface sites, surface area, surface site density, surface capacitance), have been developed to account for Fe oxyhydroxide sorption behaviour under a wide variety of pH values, ionic strengths, and sorbent–to–sorbate ratios (for an introduction to SCM see Davies and Kent, 1990). Among the early works, Dzombak and Morel (1990) provide a comprehensive database of thermodynamic parameters that describe the experimentally observed sorption of a variety of anions and cations to HFO. These surface sorption reactions may proceed to complete surface coverage, and in some cases, sorption that exceeds surface site saturation can lead to surface precipitation (*e.g.* Ler and Stanforth, 2003).

More recently, research on the sorption of trace elements to Fe oxyhydroxides has focused on determining the speciation and precise molecular coordination environment (*e.g.* mono- *vs.* bi-dentate, mono- *vs.* bi-nuclear) of sorbed trace elements using synchrotron-based spectroscopic techniques (for a review see Brown and Parks, 2001). Following the application of synchrotron spectroscopy to metal sorption systems, a new class of SCM have been developed by studies that first determine the molecular mechanisms of trace element sorption, then invoke this directly observed surface

complex to describe experimental trace element sorption data (*e.g.* Peacock and Sherman, 2004a,b; Moon and Peacock, 2011, 2012, 2013). These SCM are better able to predict trace element partitioning between solution and solid compared to those based solely on macroscopic sorption experiments. By properly defining the stoichiometry of the surface complex (*i.e.* the necessary input reaction that represents the formation of the surface complex in the model), and thus its complex-specific dependence on pH, aqueous trace element concentration and surface site density, it is possible to obtain an accurate description of its formation as a function of these same parameters. In order to apply model predictions to both modern and, in particular, ancient natural systems, where pH, trace element concentrations and surface site density (*i.e.* mineral crystallinity) vary over time and space, it is increasingly desirable to constrain SCM with molecular-level information whenever possible (*e.g.* for micronutrient trace element concentrations the modern oceans, Peacock and Sherman, 2007; Sherman and Peacock, 2010).

Significant progress has been made in testing predictive models using natural Fe oxyhydroxides (*e.g.* Tessier *et al.*, 1996; Kennedy *et al.*, 2003; Lalonde *et al.*, 2007). In some cases, highly parameterized SCM may not be practical for the description of natural systems; critical information such as mineral surface area and surface site density may be difficult to determine. In these cases, lumped-process distribution coefficients, based on the Freundlich isotherm approach, are often applied. The distribution coefficient approach, which employs a linear or exponential relationship to describe the distribution of a trace element between solid and solution, benefits from simplicity and ease of execution, but, because it does not determine the speciation or coordination environment of the sorbed trace element, it cannot properly describe the formation of the surface complex and thus the sorption of the trace element as a function of the important environmental parameters (pH, trace element concentration, *etc.*). Partition coefficients derived via this approach, either experimentally or by measuring trace element concentrations in contemporaneous solids and solutions, are therefore, limited to the particular aqueous conditions (fixed pH, trace element concentration and ionic strength) present in the experiments or at the time of trace element uptake (Langmuir, 1997). Nonetheless, as we shall see below, distribution coefficient models have proven effective for the description of trace element sequestration by natural Fe oxyhydroxides, especially in marine systems (*e.g.* Feely *et al.*, 1998; Edmonds and German, 2004), and with consideration of these limitations, they have been successfully used to relate trace element concentrations recorded in Fe mineral archives to contemporaneous seawater chemistry (*e.g.* Konhauser *et al.*, 2009).

1.2.2. Iron sulfides

Like their oxide counterparts, Fe sulfide minerals are generally insoluble, and in anoxic waters and sediment porewaters where Fe^{2+} and S^{2-} (predominately as HS^- at marine pH) are present, they precipitate rapidly. Taking the form Fe_xS_y, seven stable minerals composed entirely of Fe and S have been described, of which four may be found in low-temperature aqueous and sedimentary environments: mackinawite (meta-stable,

amorphous to tetragonal FeS), pyrite (cubic FeS_2), marcasite (orthorhombic FeS_2), and greigite (cubic Fe_3S_4). Precipitation of amorphous mackinawite proceeds faster than the other phases, such that it is often considered a precursor for its more crystalline counterparts. However, mackinawite is not a strict precursor in the sense that it does not appear to experience solid-state transformation during diagenesis, but rather undergoes dissolution and re-precipitation (*cf.* Rickard and Luther, 2007). Pyrite is the most abundant Fe sulfide mineral that is stable at Earth's surface, and like Fe oxides, it's tendency to concentrate trace elements from its formation waters makes pyrite-rich sediments both an important marine trace element sink and a rich palaeo-environmental chemical archive (*e.g.* Large *et al.*, 2014).

Similar to Fe oxides, Fe sulfide minerals present a reactive surface upon which significant trace element sorption may occur. In the case of disordered mackinawite, the reactive surface appears composed of strongly acidic mono-coordinated sulfur sites ($>FeSH^0$) and weakly acidic tri-coordinated sulfur sites ($>Fe_3SH^0$), with a specific surface area of ~350 $m^2\ g^{-1}$ (Wolthers *et al.*, 2005). Few thermodynamic surface stability constants exist for trace elements at Fe sulfide mineral surfaces, however, partition coefficients for the adsorption of metal-sulfide forming elements to the mackinawite surface appear to scale with the solubility products of their respective metal sulfides (Morse and Arakaki, 1993). Despite mackinawite being an unstable phase, the linear free-energy relationship that characterizes its trace element uptake appears reflected in the trace element compositions of sedimentary pyrites.

In pyrite-bearing marine sediments, the degree of trace element pyritization (DTMP), defined for any given trace element as the percent of that metal in a sediment that is found in pyrite (Raiswell and Canfield, 1998), also appears to scale with the respective metal sulfide solubility products (Morse and Luther, 1999; Fig. 1). In other words, the more pyrite a sediment contains, the greater the proportion of the total trace element load will be hosted in pyrite. However, not all metals display this

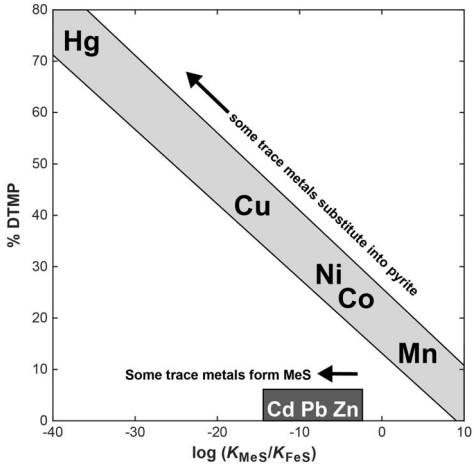

Figure 1. The degree to which different trace elements in anoxic sediments are concentrated in pyrite (% DTMP) vs. their own solubility as a metal sulfide (relative to FeS; log K_{MeS}/K_{FeS}). This relationship speaks to the affinity of different metals for sulfide as well as the kinetics of MeS *vs.* FeS precipitation. Some metals precipitate slowly as sulfides and thus are more likely to be found substituted into pyrite in anoxic sediments (metals on the pyritization trend), whereas others rapidly form their own metal sulfides and fall off this trend (Pb, Zn, Cd). Redrawn from Morse and Luther (1999).

thermodynamically-controlled behaviour; for those which may rapidly precipitate as their own amorphous metal sulfide, notably, lead (Pb), zinc (Zn), and cadmium (Cd), the kinetics of water exchange are faster than that of Fe^{2+}, and these elements tend to form their own metal sulfide phases in pyritised sediments, and DTMP for these elements remains low (Morse and Lurther, 1999). As a consequence, sedimentary pyrite is generally considered an important sink for arsenic (As), mercury (Hg), and molybdenum (Mo), moderately important for cobalt (Co), copper (Cu), manganese (Mn), and nickel (Ni), but generally unimportant for Pb, Zn, and Cd (Huerta-Diaz and Morse, 1992).

While predictive techniques, such as partition coefficient and SCM model calculations, are relatively undeveloped compared to those advanced for Fe oxide minerals, trace element concentrations in sedimentary pyrite nonetheless appear to scale with aqueous concentrations in their local environment, such that pyrite-rich sediments (*e.g.* black shales) represent a rich archive of information on Earth's surface geochemical evolution (section 3.3). Indeed, focusing on just pyrite grains from shales, Large *et al.* (2014) documented the temporal variability of several trace elements, including Mo, Co, Ni, As and Se, throughout geological time. Those authors suggested that in the same way that hydrothermal pyrite tracks the chemistry of ore-forming fluids (Large *et al.*, 2009), sedimentary pyrite can be used to track changes in seawater composition, and ultimately the redox state of Earth's surface environment. This view has recently found support in the work by Swanner *et al.* (2014) who provided pyrite, shale, and BIF trace element data that all suggested an expansion of the palaeo-marine Co reservoir between 2.48 and 1.84 Ga, coincident with anoxic marine conditions and expanded hydrothermal activity. Similarly, Gallagher *et al.* (2015) recently reported a suite of trace element data from Precambrian to Ordovician carbonate-hosted pyrites centred around several key geological events such as the Great Oxidation Event (GOE) ~2.45 Gyr (billion years ago), that were in most cases argued to be largely consistent with previous pyrite and shale records.

1.2.3. Exemplar molybdenum

Molybdenum is the most abundant transition metal in seawater (~105 nmol/kg; Anbar and Knoll, 2002) and can exist in a variety of different oxidation states depending on ocean redox. In oxic conditions, Mo is present as molybdate ($Mo(VI)O_4^{2-}$) and its concentration in seawater is though to be controlled by an equilibrium reaction in which molybdate sorbs to Fe and manganese (Mn) oxyhydroxide minerals present in ocean sediments (Barling *et al.*, 2004; Goldberg *et al.*, 2009, 2012). Under anoxic non-sulfidic conditions, where dissolved Fe is commonly present in the water column (termed ferruginous), Mo is likely drawn down in association with other minerals, such as green rust (Zegeye *et al.*, 2012). In the presence of dissolved sulfide, molybdate is converted into a series of thiomolybdate complexes, starting with oxythiomolybdates [$Mo(VI)O_{4-x}S_x^{2-}$] (when H_2S ~0.1−11 μM), which progressively dominate Mo speciation and possibly culminate in tetrathiomolybdate [$Mo(VI)S_4^{2-}$] (when H_2S >11 μM) (Helz *et al.*, 1996; Erickson and Helz, 2000). These thiomolybdates are

extremely reactive and Mo might, therefore, be drawn down via the scavenging of these complexes onto Fe minerals and sulfidized organic particles (likely at low concentrations of dissolved sulfide), or perhaps *via* the precipitation of Mo-sulfide phases (at higher concentrations of dissolved sulfide (~50–250 μM) and presumably Mo) (Helz *et al.*, 1996; Zheng *et al.*, 2000). On the other hand, these complexes might react with zero-valent sulfur present in natural sulfidic waters to produce Mo(IV)-polysulfides, which might similarly be scavenged by Fe minerals and/or organic matter (Dahl *et al.*, 2010). As such, the concentration and speciation of Mo recorded in Fe mineral archives can be used to infer prevailing ocean redox conditions at the time of sediment deposition.

Understanding how the amount of oxygen in seawater has changed through time is key to elucidating links between the evolution of ocean redox chemistry, climate and life. Oxygen provides an important control on seawater chemistry because many elements present in seawater are critically sensitive to redox conditions - existing in oxic waters either in solution as aqueous ions/organic carbon complexes or as solid forms that may be (depending on the precise chemical nature of the redox environment) sequestered into the sediments under reducing conditions. This drawdown of redox-sensitive elements, such as Mo, provides a means of reconstructing past ocean redox via careful analyses of the rock record. Indeed, the determination of Mo concentrations in marine shales is one of the most commonly used means to identify the most extreme water column redox condition (highly sulfidic, termed euxinic) throughout Earth history (Scott *et al.*, 2008).

The availability of Mo in seawater also has important implications for the biosphere because it is essential for various cellular metabolisms. For example, it is required for nitrate assimilation by eukaryotes and some prokaryotes, and its enhanced drawdown under widespread euxinic conditions in the mid-Proterozoic ocean (~1.8 Gyr) has been widely postulated as an explanation for the maintenance of low levels of atmospheric oxygen and the protracted pace of biological evolution during Earth's 'middle age' (Anbar and Knoll, 2002). As such, intimate links exist between ocean redox, biological activity, atmospheric chemistry and climate, and these can be identified and evaluated by detailed understanding of the environmental behaviour of important redox-sensitive species such as Fe and Mo.

1.3. Iron mineral archives

The most commonly utilized Fe mineral archives are those found in BIF and marine ferromanganese crusts, in which the concentrations and/or stable isotope compositions of trace elements present in the constituent Fe (and Mn) minerals can be interpreted to reflect contemporaneous seawater trace element signatures. In addition to these Fe-rich archives, scavenging of trace elements onto discrete Fe minerals, which are then deposited into marine sediments as relatively dispersed Fe phases, might also provide repositories for contemporaneous trace element seawater signatures. Indeed, trace element enrichment in black shales, which provide an important archive for redox-sensitive trace elements (*e.g.* Arnold *et al.*, 2004; Scott *et al.*, 2008), probably results

from the scavenging of particle reactive trace element species by Fe minerals (*e.g.* Helz *et al.*, 1996; Zheng *et al.*, 2000; Dahl *et al.*, 2013).

1.3.1. Banded iron formations

Banded iron formations represent vast quantities of Fe-rich sediments that were precipitated in the oceans between ~3.8 and 1.8 Ga. Trace element signatures recorded in BIF can therefore provide information on contemporaneous seawater chemistry during early Earth evolution. The name BIF stems from the appearance of these enigmatic deposits, composed of alternating bands of Fe-rich (~20−40% Fe) and silica (Si)-rich (~40−50% SiO_2) layers. Banding can often be observed on a wide range of scales, from coarse macrobands (metres in thickness) to mesobands (centimetre-thick units) to millimetre and submillimetre layers. Among the latter is the wide variety of varve-like repetitive laminae, known as microbands (Trendall and Blockley, 1970). The mineralogy of BIF from the best preserved successions is remarkably uniform, comprising mostly quartz (in the form of chert), magnetite, hematite, Fe-rich silicate minerals (stilpnomelane, minnesotaite, greenalite and riebeckite), carbonate minerals (siderite, ankerite, calcite and dolomite), and minor sulfides (pyrite and pyrrhotite); the presence of both ferric and ferrous minerals give BIF an average oxidation state of $Fe^{2.4+}$ (Klein and Beukes, 1992). However, it is generally agreed that none of the minerals in BIF are primary in origin. Instead, the minerals reflect significant post-depositional alteration under diagenetic and metamorphic conditions (including, in some cases, post-depositional fluid flow). The effect of increasing temperature and pressure is manifested by the progressive change in mineralogy through replacement and recrystallization, increase in crystal size and obliteration of primary textures (Klein, 2005). For instance, the alternating layers of magnetite and hematite are interpreted to have formed from an initial Fe oxyhydroxide phase, *e.g.* ferrihydrite, that precipitated in the photic zone when dissolved Fe^{2+} was oxidised and hydrolysed to insoluble ferric Fe. The Fe oxyhydroxide particles then sank through the water column and were deposited on the seafloor where they eventually formed (1) magnetite or Fe carbonates when organic remineralisation was coupled with Fe(III) reduction; (2) hematite, when organic material was lacking; or (3) Fe silicates, possibly in the form of a precursor mineral such as greenalite, when Si-sorbed ferric oxyhydroxides reacted with other cationic species in the sediment pore waters (Morris, 1993). The chert is widely considered to have precipitated from the water column as colloidal Si co-precipitated with Fe-rich particles (Fischer and Knoll, 2009) given that the Archaean ocean had significantly elevated concentrations of dissolved Si, at least as high as at saturation with cristobalite (0.67 mM at 40ºC in seawater), and possibly even amorphous Si (2.20 mM) (Siever, 1992; Maliva *et al.*, 2005; Konhauser *et al.*, 2007).

There is still considerable effort towards understanding how BIF formed but almost all researchers now agree that BIF were precipitated from a predominantly anoxic water column (*e.g.* Holland, 1984). The duration of BIF deposition spans major evolutionary changes in the Earth's surface composition, from an early anoxic atmosphere dominated by CO_2 and CH_4 to an atmosphere that became partially oxygenated.

Therefore, it is likely that BIF formed *via* different mechanisms throughout the Precambrian. The traditional model of BIF precipitation assumes the oxidation of dissolved Fe(II) *via* abiotic oxidation by cyanobacterially-produced O_2 (Cloud, 1973; Klein and Beukes, 1989) and/or biotic oxidation by chemolithotrophic bacteria (Holm, 1989; Planavsky *et al.*, 2009). Both models suggest the presence of free molecular oxygen in the Precambrian ocean and, hence, require the presence of oxygenic photosynthesis at that time of Earth history. Given the recent evidence for oxidative processes having already existed at 3.0 Gyr (Crowe *et al.*, 2013; Planavsky *et al.*, 2014), and perhaps even at 3.2 Gyr (Satkowski *et al.*, 2015), it might be plausible that O_2-driven reactions in the photic zone led to BIF deposition since the Mesoarchaean. An alternative biological mechanism, and one that might explain BIF deposition prior to the Mesoarchaean, involves Fe(II) oxidation *via* anoxygenic photosynthesis (Czaja *et al.*, 2013; Jones *et al.*, 2015; Pecoits *et al.*, 2015). Phototrophic Fe(II)-oxidizing bacteria were discovered two decades ago (*e.g.* Widdel *et al.*, 1993), and their metabolism involves light-energy fuelled CO_2 fixation coupled to the microbial oxidation of Fe^{2+}. The attractiveness of this concept is that it explains BIF deposition in the absence of molecular oxygen using the abundant availability of Fe^{2+}, light and CO_2 at that time (Garrels *et al.*, 1973; Hartman, 1984; Konhauser *et al.*, 2002). It has even been demonstrated by eco-physiological lab experiments in combination with modelling that these phototropic bacteria would have been capable of oxidizing enough Fe(II) to explain the large expansion of BIF deposits (Kappler *et al.*, 2005). There is in addition one abiological mechanism, that being ultraviolet photo-oxidation of Fe^{2+} in the surface waters (*e.g.* Braterman *et al.*, 1983). However, this view has been challenged on the basis that those early experiments were not conducted in complex solutions mimicking seawater (Konhauser *et al.*, 2007). Whatever the mechanism for their precipitation, BIF today have undergone probably repeated episodes of diagenesis and metamorphism, and their Fe mineralogy is now dominated by magnetite and hematite (for reviews on BIF deposition and mineralogy see Klein, 2005 and Bekker *et al.*, 2010).

1.3.2. Ferromanganese crusts

Marine ferromanganese crusts are found throughout the world's oceans and are formed of subequal amounts of Fe(III) oxyhydroxide and Mn(III,IV) minerals that have precipitated from seawater and deposited as pavements and coatings on submarine rock outcrops and topographic highs (*e.g.* Glasby, 1977). Crusts are arguably the slowest growing geological precipitates, with only a few mm deposited per million years (Ma) (*e.g.* Hein *et al.*, 2000). Accordingly, crust formations of ~10 cm thickness can provide trace element archives stretching over the last ~65 Ma of Earth history. Because ferromanganese crusts precipitate directly from ambient seawater (termed "hydrogenetic") these archives can be interpreted to reflect contemporaneous seawater chemistry throughout the Cenozoic. Crusts are restricted to submarine rock outcrops and topographic highs because these environments are often kept sediment free, *via*, for example, local currents generated by obstructional upwelling along seamount flanks.

These currents also promote enhanced turbulent mixing and upwelling, leading to increased primary productivity and development of an oxygen-minimum zone (OMZ) that increases the concentrations of Fe^{2+} and Mn^{2+} which can be scavenged into crusts during oxic conditions resulting from turbulence (Muios *et al.*, 2013). As a result of these conditions, Fe and Mn oxyhydroxides precipitated from seawater can deposit onto the hard rock surfaces and build up in layers over time, as opposed to elsewhere in the oceans where the same precipitates are deposited and dispersed into seafloor sediments. Coupled sorption and redox reactions occurring between dissolved trace elements present in contemporaneous seawater and the mineral precipitates then sequester metals as the minerals precipitate (via co-precipitation and structural incorporation) and during their transit through the marine water column (*via* adsorption onto mineral surfaces) (for a general model of crust formation see Koschinsky and Halbach, 1995). Rare and critical trace elements in particular are often concentrated to economically valuable concentrations in marine ferromanganese crusts, making the deep-sea mining of crusts and nodules a potentially attractive endeavour (*e.g.* Hein *et al.*, 2013).

The Fe mineralogy of crusts is dominated by ferrihydrite, with older crust layers sometimes featuring small (< 10%) amounts of goethite, typically attributed to aging of the authigenic ferrihydrite (*e.g.* Hein *et al.*, 2000), or a switch in precipitation from authigenic ferrihydrite to goethite during a temporary change in palaeo-seawater conditions (*e.g.* Koschinsky *et al.*, 1997). Manganese mineralogy is dominated by poorly crystalline phyllomanganates, namely δ-MnO_2 (often termed vernadite) and birnessite (*e.g.* Burns and Burns, 1977). Minor quartz, feldspar and other detrital minerals, along with sometimes significant (~20%) carbonate fluorapatite in older crusts subject to diagenesis and/or precipitated during palaeo-seawater transition, are also present (*e.g.* Hein *et al.*, 1993).

Marine ferromanganese nodules are also prevalent in the deep oceans, and, despite their similarly slow growth rates, they do accumulate and comprise a significant component of some marine and freshwater sediment. For instance, in the Pacific Ocean, it has been estimated that 10^{12} tons of nodules exist, predominantly in pelagic sediments, with an annual rate of formation of 6×10^6 tons (Mero, 1962), while in Oneida Lake, New York, for example, within a 20 km^2 area of lake, 10^6 tons of nodules, that average 15 cm in diameter, exist at the bottom sediment (Dean and Greeson, 1979). Diagenetic nodule formation involves a series of microbially-catalysed reactions. The process begins with cyanobacterial and algal plankton concentrating Fe^{2+} and Mn^{2+} from solution. Upon their death the microbial biomass and those bound metals are transported to the bottom sediment where anaerobic respiratory processes in the suboxic layers liberates Fe^{2+} and Mn^{2+} back into the sediment pore waters. Concurrently, reduction of particulate ferric oxyhydroxides and Mn(III,IV) oxides occurs. Upward diffusion to the sediment–water interface facilitates microbial re-oxidation and incorporation of metals onto some form of nucleus, which can be any solid mineral or organic substrate. With continued accretion of Fe and Mn, a nodule, that may or may not display concentric laminations, forms. Plankton contributes to

metal oxidation by producing high-pH, oxygenated surface waters that are conducive to the re-oxidation (and hydrolysis) reactions (*e.g.* Richardson *et al.*, 1988). Because nodules grow at the sediment–water interface (termed 'diagenetic') it is difficult to determine to what extent their trace element signatures reflect contemporaneous seawater chemistry and their use as archives of seawater chemical information is somewhat limited.

1.3.3. Black shales

Shales are an example of marine sediments that, although not technically classed as Fe mineral archives, can never-the-less record contemporaneous trace element seawater signatures, likely as a result of trace element drawdown in association with Fe (and sulfide and organic) phases (*e.g.* for Mo, Helz *et al.*, 1996; Zheng *et al.*, 2000; Dahl *et al.*, 2013). They comprise fine-grained clastic sediments predominantly composed of clay minerals (*e.g.* kaolinite, montmorillonite and illite) and silt-sized fragments of other minerals (*e.g.* quartz and calcite). Shales are typically grey in colour, but addition of variable amounts of minor constituents can significantly alter their appearance; most notably perhaps in the case of black shales which contain > 1% unoxidized carbonaceous material, and display an Fe mineralogy dominated by amorphous Fe sulfides and pyrite (for a summary of the geochemistry of black shale deposits see Vine and Tourtelot, 1970). This relatively high unoxidized carbon content and the presence of Fe sulfides suggests that black shales were deposited under an anoxic water column, where organic carbon was not subject to aerobic oxidative degradation and ferrous Fe was thermodynamically stable. The presence of sedimentary fabrics also indicates a lack of physical disruption by burrowing animals (at least since the Neoproterozoic). This, combined with depositional occurrences that span most of the geological record (*e.g.* Tourtelot, 1979), means that trace element signatures recorded in black shale archives can represent seawater chemistry during episodes of ocean anoxia occurring throughout Earth history.

2. Stable isotope fractionation of trace elements

Subtle physicochemical discrimination between the different stable isotopes of any given element may impart a robust geochemical fingerprint of the processes that the element has experienced, making stable isotope geochemistry a powerful tool for palaeo-environmental reconstruction. This has been recognized and exploited by geochemists for over 60 years, with early studies naturally focusing on the stable isotopes of lighter elements (H, C, N, O and S) whose greater relative mass differences imparted stronger, more easily measured fractionations. These 'traditional' stable isotope systems have since been supplemented by 'non-traditional' ones whose smaller natural fractionations have now become accessible due to advances in mass spectrometry technology. Natural stable isotope variability has now been described and quantified for an increasing number of non-traditional elements, including Li, B, Mg, Si, Cl, Ca, V, Cr, Fe, Ni, Cu, Zn, Ge, Se, Mo, Cd, Sn, Ce and Eu, and the list continues to grow (see Johnson *et al.*, 2004 dedicated to the subject).

2.1. Stable isotope nomenclature and conventions

Most stable isotope data are reported in delta notation where the isotope composition of a sample is defined as the relative deviation of the sample isotope ratio to the same isotope ratio in a known reference material (*e.g.* O'Neil, 1986):

$$\delta^{i/j}E = 1000\left(\frac{R_{i/j}\quad \text{Sample}}{R_{i/j}\quad \text{Reference}} - 1\right) \tag{2}$$

where i and j are the particular isotopes used in ratio R of element E. Units for $\delta^{i/j}E$ are in parts per thousand, *i.e.* per mil (‰). For the traditional stable isotope systems (H, C, N, O and S), the isotope ratio $R^{i/j}$ is expressed as the abundance of the minor isotope over the abundance of the major isotope, for example, D/H and $^{13}C/^{12}C$. This convention has ensured a consistent point of reference for traditional stable isotope enrichments and depletions, where a positive or negative value of $\delta^{i/j}E$ indicates that a sample is relatively enriched or depleted in the heavy isotope, respectively, compared to the standard. For several non-traditional stable isotope systems, however, $R^{i/j}$ expressed as rare over major isotope does not satisfy the heavy over light convention, because the minor isotope is the isotopically light. This is the case for the Fe and Mo stable isotope systems, where, for example, ^{54}Fe and ^{95}Mo are more rare than ^{56}Fe and ^{98}Mo. In order for stable isotope enrichments and depletions to be expressed in the same direction (heavy enrichments as positive delta values, light enrichments as negative delta values) between traditional and non-traditional systems, in non-traditional systems the convention heavy over light is usually preferred. Considering ^{54}Fe and ^{56}Fe and ^{95}Mo and ^{98}Mo, for the Fe and Mo stable isotope systems, respectively, $R^{i/j}$ is typically expressed as $^{56}Fe/^{54}Fe$ and $^{98}Mo/^{95}Mo$, with corresponding delta notation of $\delta^{56}Fe$ and $\delta^{98}Mo$.

For traditional stable isotope systems the choice of reference material for each isotope system has been internationally standardized, where, for example, the reference used for reporting the isotope compositions of H and O is Standard Mean Ocean Water (SMOW), and Air for N. For some of the non-traditional systems the reference material is yet to be agreed upon and is therefore not standardized across the field. In more recent work, Fe stable isotope measurements are usually expressed with reference to the isotope composition of the international standard IRMM-14 (Belshaw *et al.*, 2000), however, for the Mo system an international standard has only recently been proposed (NIST SRM 3134; Wen *et al.*, 2010; Greber *et al.*, 2012), and the Mo isotope community has employed various in-house Mo isotope standards over the years to normalize results (for an inter-comparison see Goldberg *et al.*, 2013). In many non-traditional stable isotope systems there is also a choice of isotope ratios that can be measured, because several of the non-traditional elements have multiple naturally occurring stable isotopes. For example, Fe has four naturally occurring stable isotopes ^{54}Fe (5.84%), ^{56}Fe (91.7%), ^{57}Fe (2.12%) and ^{58}Fe (0.28%), where stable isotope data is commonly reported as $^{56}Fe/^{54}Fe$, while Mo has seven naturally occurring stable isotopes ^{92}Mo (14.84%), ^{94}Mo (9.25%), ^{95}Mo (15.92%), ^{96}Mo (16.68%), ^{97}Mo (9.55%), ^{98}Mo (24.13%) and ^{100}Mo (9.63%), and stable isotope data has been reported

for both $^{97}Mo/^{95}Mo$ and $^{98}Mo/^{95}Mo$. As both the reference material, *REF*, and the stable isotopes measured in $R^{i/j}$ can be different for the same non-traditional stable isotope system, care is required when comparing $\delta^{i/j}E$ values between different studies. For an extended review of stable isotope nomenclature and conventions the reader is directed to Johnson *et al.* (2004).

2.2. Stable isotope fractionation theory

2.2.1. Mass-dependent stable isotope fractionation

Mass-dependent stable isotope fractionation refers to any physical or chemical process that acts to partially separate stable isotopes of the same element between two different reservoirs, where the amount of separation scales in proportion with the difference in the masses of the isotopes. For example, using the O stable isotope system, the mass difference between ^{18}O and ^{16}O is +2, while the mass difference between ^{18}O and ^{17}O is +1, so considering the partitioning of O isotopes between two different reservoirs, $\delta^{18}O$ will be approximately twice that of $\delta^{17}O$ as the result of mass-dependent fractionation. Separation of stable isotopes of the same element between two different reservoirs, and thus two separate substances, occurs because chemical bond strengths are mass-dependent. In the case of the two most abundant isotopes of O, ^{18}O and ^{16}O, in an H_2O molecule, there is a difference in bond strength between $^{18}O-H$ and $^{16}O-H$. Specifically, $^{18}O-H$ has a lower vibrational frequency, and hence a lower ground state energy (or zero point energy, ZPE), than $^{16}O-H$. This means that the bond between $^{18}O-H$ is stronger than that between $^{16}O-H$. Differences in chemical bond strength lead to differences in reaction rate constants, where species with the stronger bonds will react more slowly than species with the weaker bonds. This effect on reaction rate constants is the origin of kinetic isotope fractionation, which acts to separate isotopes during unidirectional or incomplete processes, perhaps best illustrated during evaporation of water where light water molecules (with ^{16}O) will evaporate more rapidly than heavier water molecules (with ^{18}O). Differences in chemical bond strength also lead to differences in equilibrium constants for reactions that are otherwise identical. This is the origin of equilibrium isotope fractionation, involving the partial separation of isotopes between two substances that are in chemical equilibrium. The theory of stable isotope fractionation pre-dates the advent of multi-collector inductively coupled plasma mass spectrometry (MC-ICP-MS) and the subsequent discovery of stable isotope fractionation in the heavy trace elements, and includes a few very early studies (Lindemann and Aston, 1919; Lindemann, 1919; Urey and Greiff, 1935). The modern theoretical basis for calculating mass-dependent fractionation was established over 60 years ago in a series of seminal studies by Harold Urey, Jacob Bigeleisen and Maria Mayer (*e.g.* Urey, 1947; Bigeleisen and Mayer, 1947). A rigorous treatment of mass-dependent stable isotope theory can be found in several texts, including a more recent review of fractionation fundamentals by Criss (1999).

Equilibrium stable isotope fractionation describes the partial separation of isotopes between two or more substances that are in, or are approaching, chemical equilibrium. There are a number of general qualitative chemical rules governing equilibrium stable

isotope fractionations which can be used to predict the magnitude and direction of isotope fractionation between two separate substances (for a complete review see Schauble, 2004). In the first instance, equilibrium isotope fractionations usually decrease as temperature increases, and, all else being equal, fractionations are largest for light elements and for isotopes with very different masses (*e.g.* Criss, 1999; Schauble, 2004). In addition to these rules, a further consideration of equilibrium thermodynamics provides a means to predict which substances will be enriched in heavy isotopes in a given geochemical system. In equilibrium thermodynamics, all systems strive to achieve their lowest energy state. Because chemical bonds involving heavier isotopes have a lower ground state energy than otherwise identical bonds involving lighter isotopes of the same element, then during equilibrium isotope fractionation the heavy isotope will tend to concentrate in the substance that confers the lowest ground state energy for that particular bond, *i.e.* in the substance that confers the strongest bonding environment. This process is well demonstrated in the isotope exchange of ^{18}O and ^{16}O between liquid water and water vapour:

$$H_2^{16}O\ (l) + H_2^{18}O\ (g) = H_2^{18}O\ (l) + H_2^{16}O\ (g) \quad (3)$$

where at, or approaching, chemical equilibrium, ^{18}O will concentrate in the stronger O−H bonds of water relative to the weaker O−H bonds of steam. The formation of strong bonding environments, *i.e.* strong chemical bonds, correlates with several physicochemical properties, including high oxidation state in the element of interest and low coordination number (for a full list see Schauble, 2004). Thus with a choice of bonding environment between substance *A* with element *E* in low oxidation state, and substance *B* with element *E* in high oxidation state, the heavier isotopes will tend to concentrate in substance *B*, all else being equal. Similarly, with a choice of bonding environment between substance *A* with element *E* in high coordination, and substance *B* with element *E* in low coordination, the heavier isotopes will again tend to concentrate in substance *B*, all else being equal. Overall, the general rules for equilibrium isotope fractionation predict that large equilibrium fractionations are most likely to occur at low temperature between substances with significantly different oxidation states, coordination numbers, bonding partners and/or electronic configurations (Schauble, 2004). Furthermore, these rules suggest that stable isotope signatures of redox-active trace elements, preserved in the sedimentary record, can provide a record of the palaeo redox conditions present in the environment during the time of sediment deposition. Specifically, the extent of the measured fractionation in the sedimentary record should reflect the extent of oxidation/reduction of that redox-active species in the depositional system, which is itself related to the overall redox state of the contemporaneous environment. In essence, this is the basis for utilizing redox-active trace element stable isotopes recorded in sedimentary archives as tracers of past redox and biogeochemical conditions.

2.2.2. Fractionation factors

The fractionation factor is a convenient quantification of the contrast in isotope compositions between two substances and is defined as (*e.g.* O'Neil, 1986):

$$\alpha_{A-B} = \frac{R_{i/j}A}{R_{i/j}B} \tag{4}$$

where A and B are two distinct substances, and $R_{i/j}A$ and $R_{i/j}B$ are the isotope ratios of the particular element of interest in substance A and B, respectively. The fractionation factor may also be cast in terms of $\delta^{i/j}E$ values:

$$\alpha_{A-B} = \frac{1000 + \delta^{i/j}E_A}{1000 + \delta^{i/j}E_B} \tag{5}$$

A fractionation factor of 1 indicates that the isotopes of element E are distributed evenly between substances A and B and there is no isotope fractionation. A fractionation factor > 1 indicates isotope ^{i}E (for non traditional isotope systems ^{i}E is usually the heavy isotope) is concentrated in substance A, while a fractionation factor of < 1 indicates isotope ^{i}E is concentrated in substance B. The fractionation factor does not allow differentiation between the physical processes that lead to different isotope compositions in different substances, and thus may reflect equilibrium or non-equilibrium isotope partitioning.

2.2.3. Processes producing isotopically distinct reservoirs

There are generally two types of process that can lead to the partial separation of isotopes between two reservoirs, namely, closed-system equilibrium and Rayleigh fractionation. Closed-system equilibrium is best illustrated by considering the slow reaction of two substances A and B, where A and B remain open to complete isotope exchange throughout the reaction. In this process the isotope composition of A and B is a function of the fraction of A remaining and the fraction of B produced. As the reaction proceeds, the shifting mass balances of A and B requires that their $\delta^{i/j}E$ values shift in order to maintain a constant offset in fractionation between A and B. As such, $\delta^{i/j}E_A$ and $\delta^{i/j}E_B$ will progress along a straight line as a function of the fraction of B produced (Fig. 2).

During Rayleigh fractionation the products of a reaction do not continue to exchange with other phases in the system, because, for example, they are constantly isolated or removed. So as the reaction proceeds, product B is in thermodynamic and isotope equilibrium with reactant A, but is then instantaneously removed from the system. In this case the isotope compositions of A and B evolve along an exponential trajectory, and because the product is progressively isolated, large changes in $\delta^{i}E$ values in the remaining components can occur (Fig. 2). An example would be the Fe isotope fractionations associated with ferrihydrite precipitating from seawater during the Precambrian, such that the BIF which formed in the water column and then settled out to the seafloor became progressively heavy in ^{56}Fe, while the residual Fe(II) pool in solution became isotopically more depleted (*e.g.* Rouxel *et al.,* 2005).

In addition to changes in the redox conditions of the contemporaneous environment and changes in the biogeochemical processes that ultimately control the source and sink fluxes of trace elements to and from the oceans, there are a number of independent

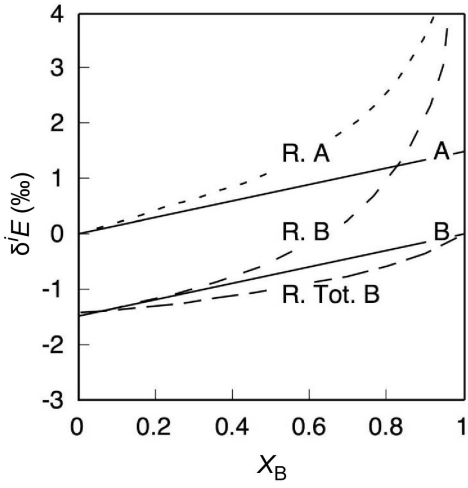

Figure 2. Comparison of the stable isotope fractionation produced by closed-system equilibrium *vs.* Rayleigh fractionation processes, during reaction of substance *A* to substance *B* with a fractionation factor α_{A-B} of 1.0015, as a function of the proportion of *B* produced (X_B). The solid lines labelled A and B reflect the isotopic evolution of the reactant *A* and product *B* during closed-system fractionation, where isotopic equilibrium is maintained. The dashed lines labelled R. A and R. B reflect the isotopic evolution of the reactant *A* and instantaneous product *B* during Rayleigh fractionation, where the product *B* is immediately isolated from isotopic exchange with reactant *A* after its formation. The dashed line labelled R. Tot. B shows the isotopic fractionation for the total product *B* during Rayleigh fractionation. Adapted from Johnson *et al*., 2004.

physicochemical processes that occur in seawater and which, according to the general rules governing equilibrium stable isotope fractionation (section 2.2.1), should be expected to cause stable isotope fractionation of trace elements and thus affect the isotope signal recorded in oceanic sedimentary archives. The first concerns the fact that almost all dissolved trace elements in seawater have varied speciation chemistry involving both inorganic and organic ligands. Physicochemical differences between the different dissolved aqueous species of element *E* in seawater, including differences in redox state, coordination number, bonding partners and electronic configurations, are expected to induce stable isotope fractionation of *E* between the relevant aqueous reservoirs (section 2.2.1). Isotope fractionation between different aqueous species have been studied for several trace element stable isotope systems, including Fe and Mo (*e.g.* Anbar *et al.*, 2000; Roe *et al.*, 2003; Welch *et al.*, 2003; Anbar *et al.*, 2005; Tossell, 2005; Weeks *et al.*, 2007). Secondly, because there can be differences in coordination number and bonding partners (*i.e.* bonding environment) between the dissolved aqueous species of *E* in seawater and the inorganic and organic particulate phases that sequester *E* into the sediments, more often than not, the act of sequestration itself can induce an isotope fractionation. In particular the stable isotope fractionation of trace elements upon sorption to Fe and Mn oxyhydroxides has been measured for Mo (Barling and Anbar, 2004; Kashiwabara *et al.*, 2011; Wasylenki *et al.*, 2011), for Ni (Wasylenki *et al.*, 2015), for Cu and Zn (Pokrovsky *et al.*, 2005; Balistrieri *et al.*, 2008; Pokrovsky *et al.*, 2008) and for Cd (Wasylenki *et al.*, 2014). In addition, for Fe and Mn oxyhydroxides in particular, sorption of element *E* can be coupled with its oxidation and the concomitant reductive dissolution of the sorbent mineral phase (*e.g.* for chromium (Cr), Manceau and Charlet, 1992; for Tl, Peacock and Moon, 2012). According to the rules governing equilibrium stable isotope fractionation, this redox

reaction can also be expected (*e.g.* for Cr, Schauble *et al.*, 2004), or in select systems has in fact been shown (*e.g.* for Tl, Peacock and Moon, 2012; Nielsen *et al.*, 2013), to induce stable isotope fractionation of *E* during sequestration to the sediments. Despite a number of studies now documenting trace element stable isotope fractionation occurring during sorption to sedimentary mineral phases, relatively few seek to determine the molecular mechanism(s) responsible for the fractionation, and thus provide a fundamental framework for understanding, interpreting and predicting fractionations between palaeo-seawater and contemporaneous trace element sedimentary archives (notable exceptions include, for Mo, Wasylenki *et al.*, 2011; for Ni, Wasylenki *et al.*, 2015; for Cu and Zn, Juliot *et al.*, 2008; Pokrovsky *et al.*, 2008; Little *et al.*, 2014; for Tl, Peacock and Moon, 2012). These studies are crucial for understanding the isotope signals measured in ancient sedimentary archives and subsequently how these archives relate to contemporaneous seawater. In particular, the isotope fractionation of trace elements during sequestration can be the dominant isotope effect in the modern oceans; for example, ferromanganese-rich sediments are known to be the main sedimentary sink for Mo in modern seawater, and during sorption to ferromanganese minerals, light Mo is preferentially sequestered leaving seawater with a heavy isotope signature of 2.3‰; this sequestration process controls the modern global Mo isotope seawater composition (*e.g.* Barling *et al.*, 2001; Siebert *et al.*, 2003; Barling and Anbar, 2004). Similar sequestration processes are also likely to be important in controlling the global seawater isotope compositions of a range of other trace elements, which are now emerging as potentially important tracers of past biogeochemical processes (*e.g.* Cu and Zn, Little *et al.*, 2014).

Recent research now indicates that the magnitude and direction of isotope fractionation that occurs during sequestration of trace elements to Fe (and Mn) oxyhydroxide minerals is controlled by the precise molecular mechanism by which the metals are sorbed from solution (*e.g.* for Ni, Wasylenki *et al.*, 2015). This, in turn, depends on an often complex combination of geochemical, physicochemical and mineralogical factors (*e.g.* for Ni; Peacock and Sherman, 2007; Peacock, 2009; Pea *et al.*, 2010). Ultimately, isotope fractionation that occurs as a result of physicochemical processes in seawater must be considered when using sedimentary trace element isotope signals as tracers of contemporaneous seawater isotope composition and, ultimately as proxies for contemporaneous environmental conditions and processes.

2.3. Predicted and measured fractionations of trace elements in geological systems

Stable isotope fractionation of the trace elements can be predicted from the theoretical basis for mass-dependent fractionation, established by Urey (1947) and Bigeleisen and Mayer (1947). These calculations are important for the new trace element systems because they provide limits to the fractionations that we might expect to measure in nature, and are particularly useful for systems that cannot be reproduced experimentally (*e.g.* Johnson *et al.*, 2004). Several of the trace element stable isotope systems have been explored theoretically, including Fe (*e.g.* Hill and Schauble,

2008), Mo (*e.g.* Weeks *et al.*, 2007, 2008; Wasylenki *et al.*, 2008, 2011), Cr (*e.g.* Schauble *et al.*, 2004), Tl (*e.g.* Schauble, 2007), and Ce (*e.g.* Nakada *et al.*, 2013). Ideally, calculated fractionations should be verified experimentally, and this is an active research area where several groups are working with both theory and experiment to shed light on measured natural isotope values and isotope variations between reservoirs (*e.g.* for Mo, Wasylenki *et al.*, 2011; for Cu and Zn, Little *et al.*, 2014).

The Fe and Mo stable isotope systems have perhaps received the most attention in terms of theoretical studies that predict fractionation between different Fe-Fe and Mo-Mo species and experimental studies quantitatively constraining that fractionation in different Fe and Mo systems. As detailed below, both elements experience significant change in their geochemical behaviour with changes in environmental redox conditions, both are important bio-essential metals linked to modern and ancient biogeochemical cycling, and both have revealed a rich sedimentary record of evolving conditions at Earth's surface.

2.4. Emerging non-traditional stable isotope systems

2.4.1. Iron

Compared to the lower-mass traditional stable isotopes (H, C, N, O and S), fractionations for higher-mass elements are not expected to exceed 10 per mil at temperatures equal or below 100ºC (Johnson *et al.*, 2004). Unlike other more volatile isotopic systems (*e.g.* C and O), Fe isotopes are geochemically robust, retaining their environmental signature even in the face of extreme metamorphic conditions (*e.g.* Frost *et al.*, 2007; Dauphas *et al.*, 2007), making them a useful tool in deciphering the biogeochemical history of highly deformed and metamorphosed rocks.

Iron has four naturally occurring stable isotopes ^{54}Fe (5.84%), ^{56}Fe (91.7%), ^{57}Fe (2.12%) and ^{58}Fe (0.28%), where stable isotope data are commonly reported as ^{56}Fe/^{54}Fe. Many natural materials tend to have distinctively narrow δ^{56}Fe ranges, where most igneous rocks fall within the 0.00±0.05 ‰ range, as do riverine and marine sediments, shales, and modern wind-blown sediments (Beard *et al.*, 2003; Fig. 3). In contrast, Fe-rich sediments have characteristically large variations in δ^{56}Fe (Fig. 3). This large variation is interpreted to have been caused by a combination of factors, including mineral-specific equilibrium isotope fractionation, variations in the original Fe isotope composition of the fluids from which these minerals precipitated, and bacterial metabolic processes which might have influenced their formation (Fig. 4; Johnson *et al.*, 2003; 2008b). Metabolically-processed Fe may also retain a 'vital effect' due to the redox-related changes driving Fe isotope fractionation during microbially-influenced Fe mineral precipitation (Fig. 4; Johnson *et al.*, 2002).

While Fe isotope systematics has gained widespread attention in applications ranging from chemical weathering, soil formation, the formation of ore deposits, and modern marine metal cycling, their principal application to date in terms of Earth's redox and biogeochemical evolution has focused on the Precambrian record of Fe isotopes archived in BIF (section 3.1.2).

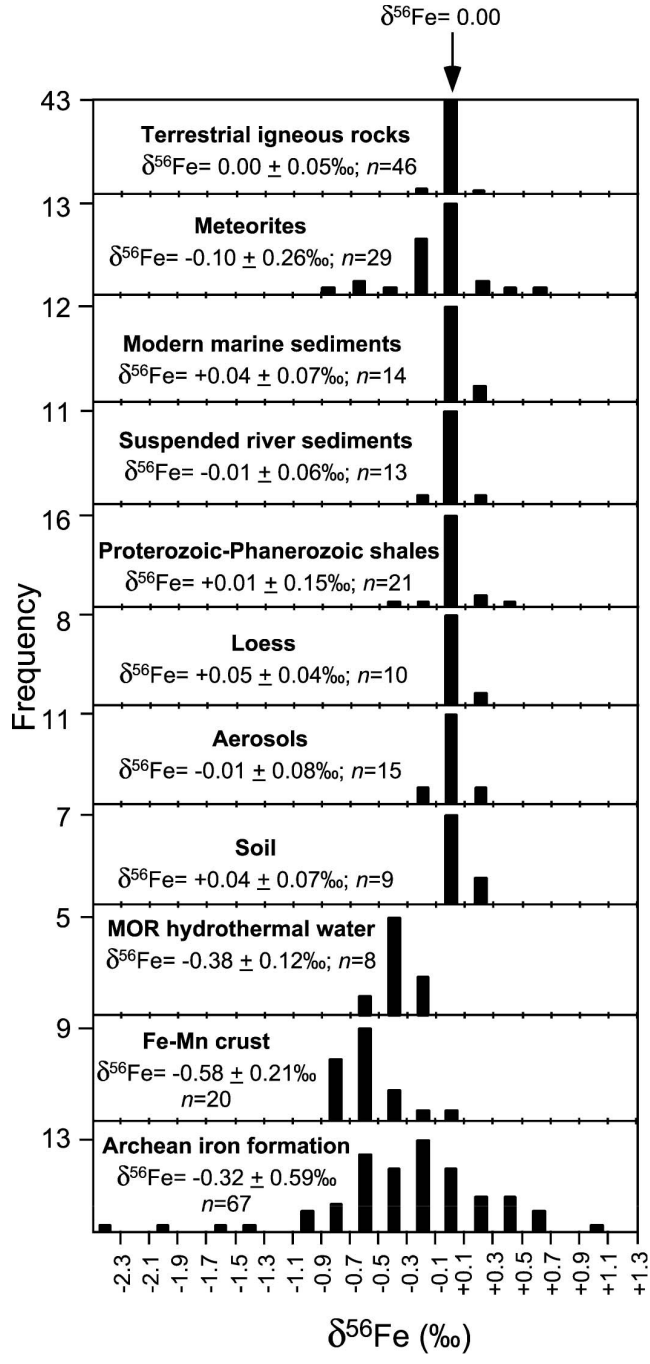

Figure 3. Iron isotope composition of natural materials. Adapted from Beard *et al*. (2003).

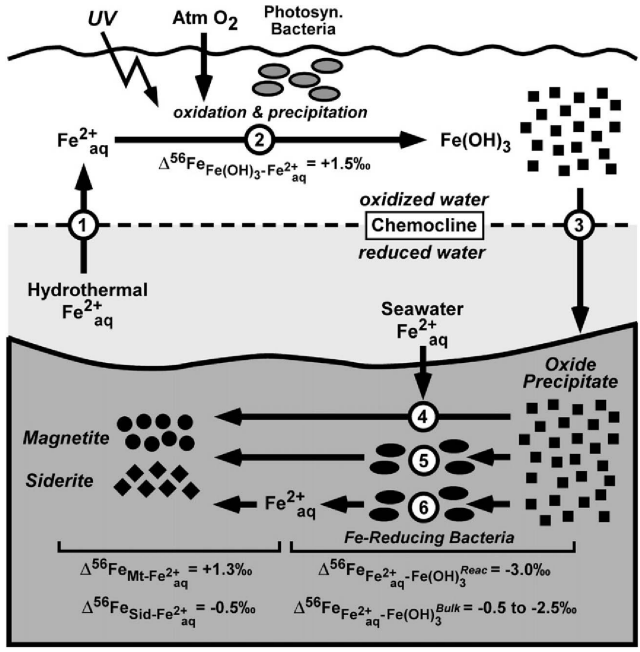

Figure 4. Pathways of iron cycling and associated isotopic fractionations during the deposition and early diagenesis of iron formation. Adapted from Johnson *et al*., 2007.

2.4.2. Molybdenum

The Mo isotope composition of modern and ancient Fe mineral archives has received significant attention due to the strong potential for palaeo-redox reconstruction (Barling *et al.*, 2001; McManus *et al.*, 2002; Siebert *et al.*, 2003; Arnold *et al.*, 2004; Barling and Anbar, 2004; Archer and Vance, 2008; Voegelin *et al.*, 2009; 2010; Planavsky *et al.*, 2014). Molybdenum has seven naturally occurring stable isotopes ^{92}Mo (14.84%), ^{94}Mo (9.25%), ^{95}Mo (15.92%), ^{96}Mo (16.68%), ^{97}Mo (9.55%), ^{98}Mo (24.13%) and ^{100}Mo (9.63%) and Mo isotopic compositions represented in the conventional δ notation have been primarily reported in two different ways in the literature. The most common reporting is $\delta^{98/95}$Mo with respect to the isotope standard "Bern-Mo" (Johnson Matthey ICP standard, lot 602332B; McManus *et al.*, 2002; Siebert *et al.*, 2003; Voegelin *et al.*, 2009, 2010). The second most common reporting is $\delta^{97/95}$Mo with respect to Roch-Mo2 (Johnson Matthey Specpure Molybdenum Plasma Standard, lot 7024991; Barling *et al.*, 2001; Barling and Anbar, 2004). Despite this apparent complexity, it is relatively easy to convert from $\delta^{98/95}$Mo to $\delta^{97/95}$Mo with a simple multiplication factor of 2/3, corresponding to the relative mass difference between these notations. The NIST SRM 3134 Mo standard has since been proposed by Greber *et al.* (2012) in order to enable easier data comparisons between studies. Goldberg *et al.* (2013) calibrated the NIST SRM 3134 standard relative to Roch-Mo2 and Bern-Mo as follows: $\delta^{98/95}Mo_{SRM\ 3134} = \delta^{98/95}Mo_{Roch\text{-}Mo2} + 0.34 \pm 0.05$ ‰ and $\delta^{98/95}Mo_{SRM\ 3134} = \delta^{98/95}Mo_{Bern\text{-}Mo} + 0.27 \pm 0.06$‰.

Siebert *et al*. (2003) were the first to constrain mean ocean $\delta^{98/95}$Mo, reporting an isotopically heavy value of 2.63‰ ± 0.1 (2SD). An even heavier isotopic composition was reported by McManus *et al.* (2002) for deep marine sediment pore waters, where isotopically light Mo (relative to seawater) accumulates in reducing sediments (the most important marine Mo sink), leaving a low concentration of heavy residual Mo in associated pore waters.

All oceanic Mo sources and sinks have a lighter isotopic composition than seawater (Fig. 5). The isotopic offset between oxic and anoxic sediments is fixed by the isotopic composition of the most important Mo source, river water, which may vary in dissolved Mo isotope composition between 0 and 2.3‰ and averages around 0.7‰ (Archer and Vance, 2008). The heavy Mo isotopic composition of seawater is largely determined by the areal extent of sediments underlying an anoxic water column, which have a light isotopic composition and are the most important marine sink of Mo (McManus *et al.*, 2002; Siebert *et al.*, 2003). The second most important sink, Fe and Mn oxide-rich sediments, represents an even lighter Mo isotope exit channel, but is less important today than the anoxic sedimentary sink (Arnold *et al.*, 2004). Thus isotopically heavier

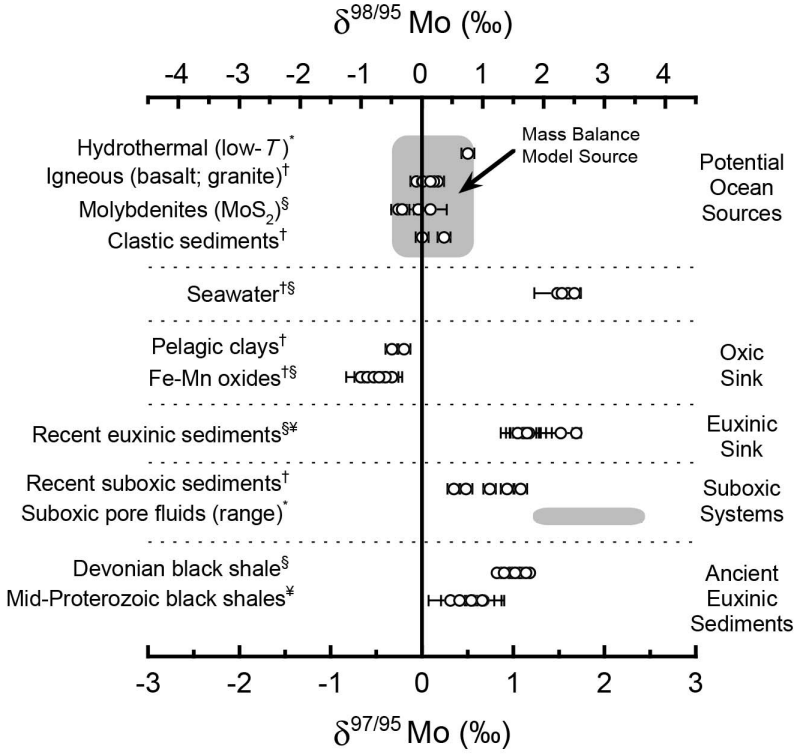

Figure 5. Mo isotope compositions of marine sediments deposited under diverse water column redox conditions. Adapted from Anbar (2004).

seawater values reflect a rigorous oxic sink removing light Mo isotopes, and isotopically lighter seawater values reflect a more important role for anoxic and euxinic sinks that sequester the heavier isotopes. Uptake of Mo into carbonates is assumed to have an insignificant effect on the Mo isotopic composition of seawater because they contain very little Mo and are thus relatively unimportant from a mass-balance perspective compared to the major sources and sinks identified.

2.4.3. Chromium

The mobile chromium(VI) anion ($HCrO_4^-$) is the most thermodynamically stable form of Cr in equilibrium with modern atmospheric oxygen. Chromium(III) is the most stable form under reduced conditions, and its mobilization is only prevalent under strongly acidic conditions. The oxidation to Cr(VI) depends upon the solubilisation of primary Cr(III)-bearing mineral phases, such as chromite ($FeCr_2O_4$), and the subsequent reaction of dissolved Cr(III) with Mn(IV) oxides (reaction 6). The latter is the only naturally occurring oxidant of Cr(III) at pH<9 (Eary and Rai, 1987), but because it requires the presence of elevated O_2 levels to oxidize Mn(II) to Mn(IV), Cr mobility is ultimately tied to environmental oxygenation. Chromium(VI) can be reduced to Cr(III) by microbes (Sikora *et al.*, 2008) and by Fe^{2+} (reaction 7) or Fe(II)-bearing minerals (Ellis *et al.*, 2002). The oxidation of dissolved Fe^{2+} by Cr(VI) proceeds on the order of minutes, and is much faster than with oxygen, even under well aerated, high-pH conditions (Eary and Rai, 1989). This means that in the presence of Fe(II), Cr(IV) is efficiently reduced to Cr(III). The Cr(III) is subsequently and effectively scavenged into Fe(III)-Cr(III) oxyhydroxides owing to the very low solubility of $(Fe,Cr)(OH)_3$ (Sass and Rai, 1987). Moreover, the formation of a solid phase greatly reduces the potential for transformation back to Cr(VI) (Fendorf, 1995).

$$Cr^{3+} + 1.5MnO_2 + H_2O \rightarrow HCrO_4^- + 1.5Mn^{2+} + H^+ \quad (6)$$

$$3HCrO_4^- + 9Fe^{2+} + 15H_2O \rightarrow 3(Fe,Cr)(OH)_3 + 6Fe(OH)_3 + 15H^+ \quad (7)$$

Chromium has four stable isotopes of masses 50 (4.35%), 52 (83.8%), 53 (9.50%) and 54 (2.37%). After Cr(III) oxidation, the Cr(VI) anion is enriched by up to 7‰ in ^{53}Cr compared to coexisting compounds containing Cr(III), leaving the aqueous phase with positive $\delta^{53}Cr$ values and the residual soils and weathered rock with negative $\delta^{53}Cr$ values (Schauble *et al.*, 2004; Zink *et al.*, 2010). This positive Cr(VI) signal should be transferred to the oceans because subsequent sorption of Cr(VI) onto soil and sediment particles apparently produces no isotope effect (Ellis *et al.*, 2004). The microbial reduction of Cr(VI) further generates isotopic shifts of up to 4.1‰, comparable to those produced during abiotic reduction (Ellis *et al.*, 2002). The overall effects of Cr redox reactions are, therefore, to enrich the heavier isotope in the remaining dissolved Cr(VI). Chemical sediments may then capture the signal of oxidative continental weathering if the Cr(VI) pool is large enough to alter the Cr isotope composition of seawater.

3. Iron-based records of Earth's redox and biogeochemical evolution

3.1. Banded iron formations

One of the unique sedimentological features of the Archaean oceans was the deposition of banded iron formation (BIF). As reviewed below, several aspects of the trace element signatures recorded in these enigmatic deposits are employed to reconstruct Earth's ancient redox and biogeochemical evolution.

3.1.1. Rare earth elements

Rare earth element (*REE*) studies in BIF focus on two central facets, namely understanding the sources of Fe to the ancient oceans, and the ancient water column redox conditions. At the heart of *REE* studies in BIF is the assumption that there is minimal fractionation of *REE* during precipitation of the primary ferric oxyhydroxides. Iron formations are, therefore, inferred to have trapped a *REE* signature of seawater at the site of Fe precipitation.

For over half of Earth's history, seawater was characterized by its high Fe concentrations, leading to the notion that the Archaean oceans (4.0–2.5 Ga) were "ferruginous" throughout much of the anoxic water column. Early studies invoked a continental source of Fe, since Fe(II) was much more mobile during weathering in the absence of atmospheric O_2 (*e.g.* James, 1954; Lepp and Goldich, 1964) and potentially since continents had a more mafic composition than today (Condie, 1993). Holland (1973) later suggested that Fe was instead sourced from deep marine waters and supplied to the depositional settings *via* upwelling. With the discovery of modern seafloor-hydrothermal systems (*e.g.* Corliss *et al.*, 1978) and the subsequent recognition that modern hydrothermal systems may contribute up to 75% of dissolved Fe to the Fe budget in the deep-oceans (Carazzo *et al.*, 2013), submarine venting has become the generally agreed upon source for seawater Fe.

Perhaps the strongest support for a submarine volcanic source for BIF comes from its europium (Eu) enrichment, which indicates a strong influence of high-temperature hydrothermal fluids on the seawater dissolved *REE* load (*e.g.* Klinkhammer *et al.*, 1983; Derry and Jacobsen, 1988, 1990). The disparate behaviour of Eu from neighbouring *REE* in hydrothermal fluids is linked with Eu(III) reduction at high-temperature and low Eh conditions (Klinkhammer *et al.*, 1983; Sverjensky, 1984). It is generally assumed that Fe and *REE* will not be fractionated during transport from spreading ridges or other exhalative centres, and, therefore, a strong positive Eu anomaly indicates that the Fe in the precursor sediment was hydrothermally derived (*e.g.* Slack *et al.*, 2007). In this regard, secular trends in the magnitude of Eu anomalies in BIF has historically been assumed to indicate variations in hydrothermal flux, with a long-term decrease in hydrothermal activity from the Eoarchean to Palaeoproterozoic (*e.g.* Huston and Logan, 2004; Sreenivas and Murakami, 2005). This *REE* trend is likely linked with an overall decline in the delivery of reductants from Earth's interior.

Neodymium (Nd) isotopes have also been shown to be highly valuable in tracing the source input of Fe to BIF. For example, a number of BIF record mixing of $^{143}Nd/^{144}Nd$ from primarily two sources: (1) anoxic deep water with generally positive initial εNd

(εNd(i)) values reflecting submarine mid-ocean ridge basalt (MORB)-like depleted sources, and (2) shallower waters with generally lower εNd(i), reflecting riverine input from evolved continental sources (*e.g.* Alibert and McCulloch, 1993; Bau *et al.*, 1997; Frei and Polat, 2007). Newly compiled $^{143}Nd/^{144}Nd$ data by Alexander *et al.* (2009) of BIF older than 2.7 Ga suggest that bulk anoxic Archaean seawater was dominated by high-temperature hydrothermal alteration of mantle-derived oceanic crust, presumably also responsible for delivering the Fe to the BIF. However, deviation from this mantle Nd signal has been recorded in the 2.9 Ga-old Pongola BIF in South Africa, which was deposited in a near-shore, shallow-water environment where continental fluxes of Fe and other solutes contributed greatly to the unit's composition (Alexander *et al.*, 2009). Similarly, Haugaard *et al.* (2013) reported positive εNd values in the Si-rich bands of the 2.9 Ga Itilliarsuk BIF of West Greenland, suggesting that those *REE* were controlled by a local, depleted continental crust, whereas the negative $\varepsilon_{Nd}(i)$ values found in the Fe-rich layers were hydrothermally-sourced. Nevertheless, from Archaean to Proterozoic, there is a gradual decrease in hydrothermal activities as the Earth cooled, and a stronger continental contribution of Nd to the ocean (Miller and O'Nions, 1985; Jacobsen and Pimentel-Klose, 1988).

Anomalies in cerium (Ce) abundance in BIF have been used to constrain water column redox conditions. In general, oxygenated marine settings display a strong negative Ce anomaly when normalized to shale composite ($Ce_{(SN)}$), while suboxic and anoxic waters lack significant negative $Ce_{(SN)}$ anomalies and can even show positive anomalies (*e.g.* German and Elderfield, 1990; Byrne and Sholkovitz, 1996). Oxidation of Ce(III) to Ce(IV) greatly reduces Ce solubility, resulting in its preferential removal onto Mn(IV)-Fe(III)-oxyhydroxides, organic matter and clay particles. In contrast, suboxic and anoxic waters lack significant negative $Ce_{(SN)}$ anomalies due to reductive dissolution of settling Mn(IV)-Fe(III)-oxyhydroxide particles. Similarly, light *REE* depletion develops in oxygenated waters due to preferential removal of light *vs*. heavy *REE* onto Mn(IV)-Fe(III)-oxyhydroxides and other particle-reactive surfaces. As a result, the ratio of light-to-heavy *REE* markedly increases across redox boundaries due to reductive dissolution of Mn(IV)-Fe(III)-oxyhydroxides (German *et al.*, 1991; Byrne and Sholkovitz, 1996). In many Archaean and early Palaeoproterozoic BIF there are no Ce anomalies, and thus no deviation from trivalent Ce behaviour (*e.g.* Alexander *et al.*, 2008; Frei *et al.*, 2008), suggesting that the water column from which ferric oxyhydroxides precipitated was anoxic (Bau and Dulski, 1996). In support of this model, a recent survey of 18 different Palaeoproterozoic and Archean BIF did not display significant Ce anomalies until after atmospheric oxygenation at ~2.5−2.4 Ga (Planavsky *et al.*, 2010a).

There also appear to be differences in trivalent *REE* behaviour in BIF before and after the permanent rise of atmospheric oxygen. Late Palaeoproterozoic BIF show significant ranges in light-to-heavy *REE* ($Pr/Yb_{(SN)}$) ratios, both below and above the shale composite value (Planavsky *et al.*, 2010a). This range of light-to-heavy *REE* and Y/Ho ratios in late Palaeoproterozoic BIF likely reflects variable fractionation of *REE* + Y by Mn(IV)-Fe(III)-oxyhydroxide precipitation and dissolution. This interpretation implies deposition of late Palaeoproterozoic BIF at ~1.9 Ga in basins with varying

redox conditions and a strong redoxcline separating an upper oxic water column from deeper waters that were suboxic to anoxic (Planavsky *et al.*, 2009). These ranges are also similar to those seen in modern anoxic basins. In contrast, most Archaean and early Palaeoproterozoic BIF deposited before the rise of atmospheric oxygen are characterized by consistent light *REE* depletion (Planavsky *et al.*, 2010a). This consistent depletion in light *REE* suggests the lack of a discrete redoxcline and points toward O_2-independent Fe(II) oxidation mechanisms.

3.1.2. Trace element isotope compositions

In addition to *REE* signatures recorded in BIF, Fe isotope signatures archived in these deposits are also used to shed light on ancient redox conditions. The primary Fe minerals that ultimately sedimented to yield BIF were probably formed in the water column as the result of oxidation of $Fe(II)_{aq}$, where overall fractionation appears to be independent of the oxidative pathway, whether by molecular oxygen, anaerobic photoferrotrophy or UV photo-oxidation (Fig. 4; *e.g.* Bullen *et al.*, 2001; Croal *et al.*, 2004; Balci *et al.*, 2006; Staton *et al.*, 2006). While complete oxidation of an $Fe(II)_{aq}$ pool will result in ferric oxyhydroxides with a $\delta^{56}Fe$ composition equal to that of the initial pool, partial oxidation will result in ferric oxyhydroxides that are up to +4‰ higher (*e.g.* Wu *et al.*, 2012). Reactions between these ferric oxyhydroxide precipitates and various $Fe(II)_{aq}$ pools as they descend through the water column and their diagenesis upon burial result in their conversion to important BIF forming minerals (*e.g.* hematite, magnetite, siderite, ankerite).

In Precambrian BIF, positive $\delta^{56}Fe$ signatures are thought to occur *via* the interaction of ferric oxyhydroxides formed by partial oxidation of hydrothermally-sourced $Fe(II)_{aq}$, with more pristine pools of hydrothermally sourced $Fe(II)_{aq}$ contributing near-zero $\delta^{56}Fe$ values. Such a scenario is easily envisioned for oxidative mechanisms restricted to the upper water column, where isotopically heavy precipitates formed in a zone of partial oxidation rain into a deeper, isotopically pristine hydrothermal $Fe(II)_{aq}$ pool. Alternatively, positive signatures may be generated *via* the partial or near-complete reduction of ferric oxyhydroxides of nearly any initial isotope composition. Dissimilatory Fe reduction (DIR) by Fe reducing bacteria releases isotopically light $Fe(II)_{aq}$ and leaves the residual oxide isotopically heavy (Fig. 4). This appears reflected in the Fe isotope composition of mineral separates from Precambrian BIF, where hematite is systematically heavier than magnetite, the latter likely formed by reaction of primary Fe oxyhydroxides with isotopically light Fe released by DIR (Johnson *et al.*, 2008a). With few electron acceptors available for anaerobic respiration in marine sediments on the O_2-poor early Earth, DIR would have probably constituted a major remineralization pathway during sedimentary diagenesis (Konhauser *et al.*, 2005). The Fe isotope record in both sedimentary pyrites and Precambrian BIF (Johnson *et al.*, 2008b) demonstrates a profound excursion to extremely negative Fe isotope values ~2.7 Ga that would appear to reflect increasingly important DIR in the run-up to Earth surface oxygenation (Fig. 6). In this model, extremely light Fe isotope compositions reflects a period in Earth's history where reduction of increasingly abundant

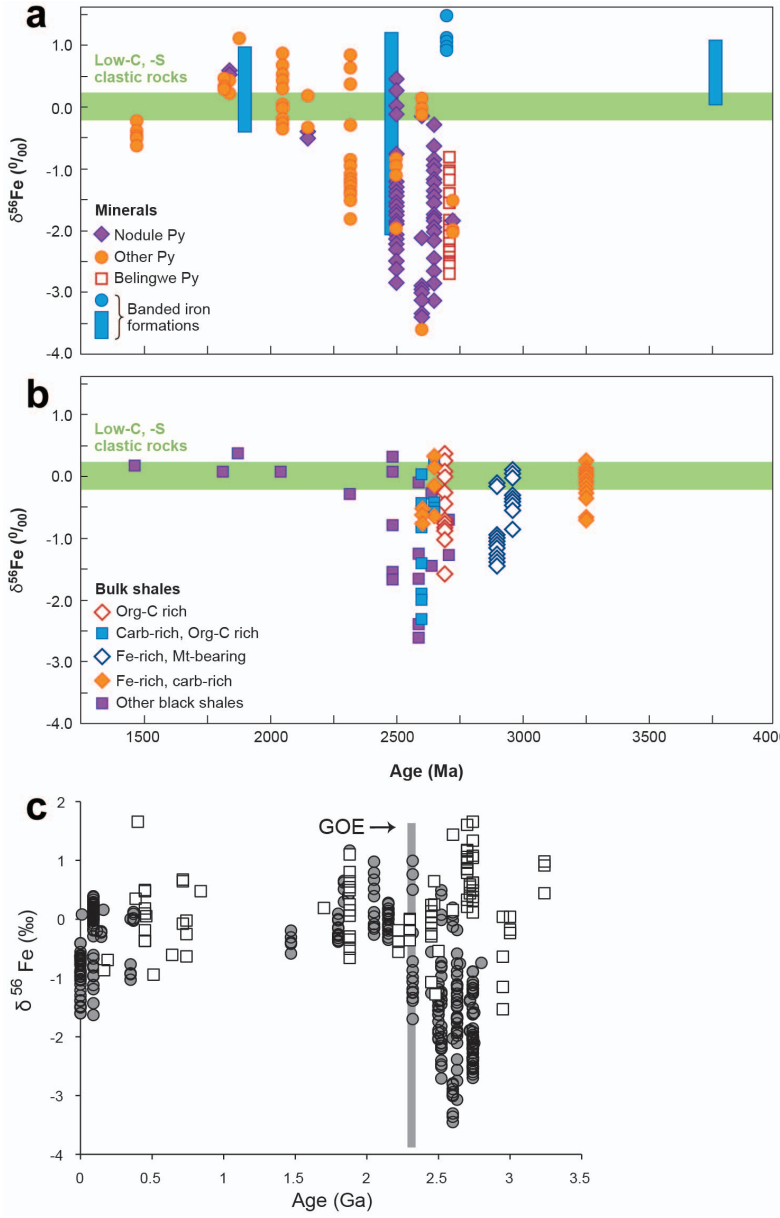

Figure 6. Iron isotope compositions of sedimentary sulfide minerals (a), iron formations (b) and whole-rock data from shales (c **Authors, correct?**) through the Archaean to Mesoproterozoic. Adapted from Johnson *et al*. (2008) and Planavsky *et al*. (2012).

sedimentary Fe oxyhydroxides was one of the most important organic carbon remineralisation pathways in deep marine settings on the O_2- and SO_4-poor early Earth.

The apparently sensitive character of Mo isotope redox proxies has also been exploited in Precambrian Fe formations in the search for the oldest traces of free O_2 on Earth. Examining a suite of Precambrian Fe formations of various ages, Planavsky *et al.* (2014) revealed a trend between Mo isotope compositions and Fe/Mn ratios (Fig. 7), with isotopically lighter Mo isotope compositions occurring as Fe/Mn decreases (and thus Mn increases). This is interpreted as a redox array where under more reducing conditions, when conditions are prohibitive to Mn(II) oxidation and Mn(III,IV) oxide deposition, Mo isotope compositions of BIF tend towards values expected for equilibrium isotope fractionation between Fe oxyhydroxides and seawater (with Mo in Fe oxyhydroxides being ~1‰ lighter than in coeval seawater); when Mn(III,IV) oxides are deposited under more oxidizing conditions, the greater equilibrium Mo isotope fractionation between Mn oxides and seawater is expressed (with Mo in Mn oxides being ~2‰ lighter than coeval seawater). Molybdenum isotope compositions as light as −0.9‰ in the 2.95 Ga Sinqeni Fe formation (Pongola Supergroup, S. Africa) could be generated only by Mo adsorption onto Mn(III,IV) oxides during deposition of this deposit; in the study of Planavsky *et al.* (2014), the Mo isotope data appear to be signalling the ancient presence of Mn(III,IV) oxides, and thus significant O_2, in the

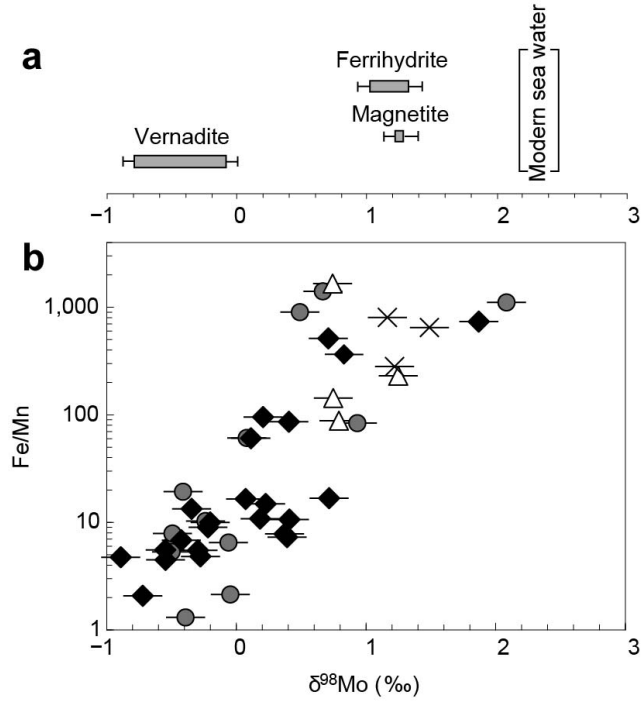

Figure. 7. Mo isotope compositions of diverse Precambrian iron formations whose trend as a function of Fe/Mn ratios indicate adsorption of Mo onto Mn oxides, and by consequence the presence of appreciable free O_2, as far back as 2.96 Ga. Adapted from Planavsky *et al*. (2014).

environment despite the fact that no Mn(III,IV) oxides are currently found in the deposit (having likely been the subject of dissimilatory Mn(III,IV) reduction, leaving the Fe formation enriched only in Mn(II)). These data are amongst Earth's earliest evidence for free O_2 in the environment, and place important constraints on the timing of the evolution of oxygenic photosynthesis. Mo isotope proxies have also been widely applied in the study of evolving marine palaeo-redox using the more extensive shale record (section 3.3.2).

3.1.3. Trace element concentrations

In natural systems where trace element sequestration by authigenic ferric oxyhydroxides results from a continuum of adsorption and co-precipitation reactions, lumped-process distribution coefficient models can be used to relate the concentration of an element in the Fe oxide to the dissolved concentration present at the time of precipitation, *i.e.* they reflect contemporaneous seawater trace element signatures. This predictive aspect of metal sorption reactions has been exploited to better understand the BIF record with respect to ancient seawater composition and nutrient limitations on Precambrian primary productivity.

The phosphorus (P) content of BIF has received significant attention as ferric oxyhydroxides possess a strong affinity for dissolved phosphate, and phosphate is a bio-essential nutrient whose availability can limit phytoplankton productivity in modern oceans. Today, particles of ferric oxyhydroxide that precipitate out of some marine hydrothermal vent fluids upon mixing with oxygenated seawater have been noted to strongly adsorb phosphate from seawater, to the point where the resulting particles attain molar P/Fe(III) ratios of over 0.2 (Feely *et al.*, 1990, 1998). Seawater phosphate concentrations at hydrothermally active spreading centres may be strongly affected by adsorption onto ferric oxyhydroxides; at the Juan de Fuca ridge for example, significant negative phosphate anomalies have been noted at depth, with phosphate declining most appreciably (by approximately 60 nM) nearest to the ridge axis, coincident with increased sediment Fe and P concentrations (Feely *et al.*, 1990). Later work by Wheat *et al.* (1996) indicated that marine hydrothermal systems annually remove about 50% of the preindustrial dissolved riverine phosphate flux, and that the co-precipitation of phosphate with ferric oxyhydroxides in seawater accounts for 36–66% of that removal rate. The extent to which phosphate is incorporated into the particles depends on the available phosphate concentration, in a manner that can be described using a distribution coefficient (K_D):

$$K_D = \frac{P/Fe(III)}{[P]} \tag{8}$$

where *P/Fe(III)* represents the particle's solid phase molar ratio, and [*P*] represents the dissolved phosphate concentration at the time of particle precipitation. Both experimental studies (Konhauser *et al.*, 2007) and field data (Feely *et al.*, 1998) demonstrate that this relationship is well described at pH ~8 by a K_D value of approximately 0.06–0.075 mM^{-1}.

Assuming that the ferric oxyhydroxides precipitates originally constituting Precambrian BIF behaved similarly, Bjerrum and Canfield (2002) applied a K_D value of 0.06 mM^{-1} to extrapolate Precambrian ocean phosphate concentrations from the concentrations of Fe(III) and P retained in BIF. Their results indicated that ocean phosphate concentrations might have been low enough (10 to 25% of present day values) to significantly limit biological productivity prior to 1.8 Ga.

Konhauser *et al.* (2007) re-examined the BIF palaeo-proxy for P by evaluating the role of Si as a ferric oxyhydroxide co-precipitate and phosphate adsorption competitor. Throughout the Precambrian, the oceans had a significantly higher concentration of dissolved Si, at least as high as at saturation with cristobalite (0.67 mM at 40ºC in seawater), and possibly even amorphous Si (2.20 mM) (Maliva *et al.*, 2005). Silica concentrations close to or at saturation with respect to amorphous Si likely persisted until the early Cretaceous, when the disappearance of VMS-associated hematitic jasper deposits indicate that diatoms or other Si-secreting organisms began actively scavenging Si (Grenne and Slack, 2003), eventually to reduce its concentration to a modern average that is less than 0.10 mM (Tréguer *et al.*, 1995). Crucially, Si strongly adsorbs to ferric oxyhydroxides and effectively competes with phosphate for available adsorption sites. This was demonstrated experimentally by Konhauser *et al.* (2007), who used a revised K_D approach accounting for Fe-Si co-precipitation indicates that with sufficiently high Si concentrations, the scavenging of phosphate by Fe-rich hydrothermal fluid precipitates is minimal (Fig. 8). The BIF P record, interpreted in this light, might indicate that phosphate was more abundant in Precambrian oceans than today. Additionally, high levels of carbonate saturation during the Precambrian (*e.g.* Grotzinger, 1990) would have inhibited carbonate fluorapatite (CFA) formation, which today is the largest burial flux for phosphorous in modern oceans (Ruttenberg and Berner, 1993). Combined, these two factors suggest higher, rather than lower dissolved Archean phosphorous concentrations. A subsequent increase in P content of BIF in the Neoproterozoic, following Snowball Earth deglaciations, may then have led to enhanced cyanobacterial photosynthesis, which in turn, produced enough oxygen to facilitate the evolution of animal life (Planavsky *et al.*, 2010b; Fig. 9a). Jones *et al.* (2015) recently re-evaluated the partitioning of P in solutions even more closely approximating seawater, and found that beyond Si, Ca and Mg can have equally important effects on P partitioning to the surfaces of Fe oxyhydroxide minerals, and the subject of calibration of adsorption-dependent Fe oxyhydroxide proxies remains an area of active investigation.

The Ni content of BIF has also received significant attention because it has been shown that Ni concentrations in BIF have changed dramatically over time, and that a drop in Ni availability in the oceans around 2.7 Ga would have had profound consequences for microorganisms that depended on it, that being methane-producing bacteria called methanogens (Konhauser *et al.*, 2009, 2015; Fig. 9b). These bacteria have a unique Ni requirement for their methane-producing enzymes, and crucially, these bacteria have been implicated in controlling oxygen levels on the ancient Earth as the methane they produced was reactive with oxygen and kept atmospheric oxygen

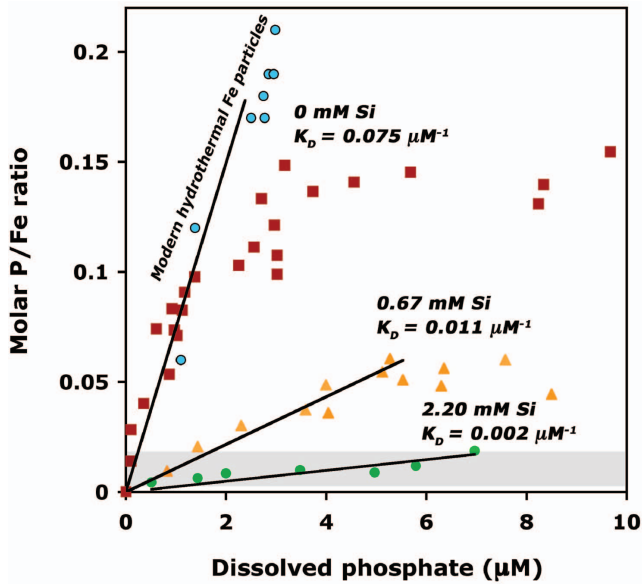

Figure 8. Experimentally-determined partitioning coefficients (K_D; black lines and bold text) for partitioning of phosphate between simulated seawater and ferrihydrite under different ambient dissolved silica conditions (red squares, orange triangles, and green circles represent 0, 0.67, and 2.2 mM dissolved Si, respectively). Also shown are data for modern hydrothermal plumes worldwide (blue circles). This experiment demonstrates that suppressed partitioning of P into iron oxyhydroxides under Precambrian marine Si concentrations may be responsible for the low P/Fe ratio of BIF (area shaded grey). Adapted from Konhauser *et al*. (2007).

levels low. It is possible that a Ni famine eventually led to a cascade of events that began with reduced methane production, the expansion of cyanobacteria into shallow-water settings previously occupied by methanogens, and ultimately increased oxygenic photosynthesis that tipped the atmospheric balance in favour of oxygen, the so-called GOE at 2.45 Ga. Perhaps it is no coincidence that at this time stromatolites expanded and diversified into shallow-water settings (McNamara and Awramik, 1992), and with increased consumption of CO_2, indiscriminate sedimentation of massive amounts of calcium carbonate took place *in situ* on the sea floor, leading to decimetre- to metre-thick beds that extended over thousands of square kilometres (Grotzinger and Knoll, 1999).

A recent compilation of Cr enrichment in BIF shows a profound enrichment coincident with the GOE around 2.45 Ga (Konhauser *et al.*, 2011; Fig. 9c). After that Cr enrichments started to increase in shallow-water BIF and peaked synchronous with the permanent loss at ~2.32 Ga of mass-independent fractionation of sulfur isotopes that defines the GOE (Bekker *et al.*, 2004, Guo *et al.*, 2009). Given the insolubility of Cr minerals, its mobilization and incorporation into BIF indicates enhanced chemical weathering at that time, most likely associated with the evolution of aerobic continental pyrite oxidation. As the GOE commenced, aerobic chemolithoautotrophic weathering

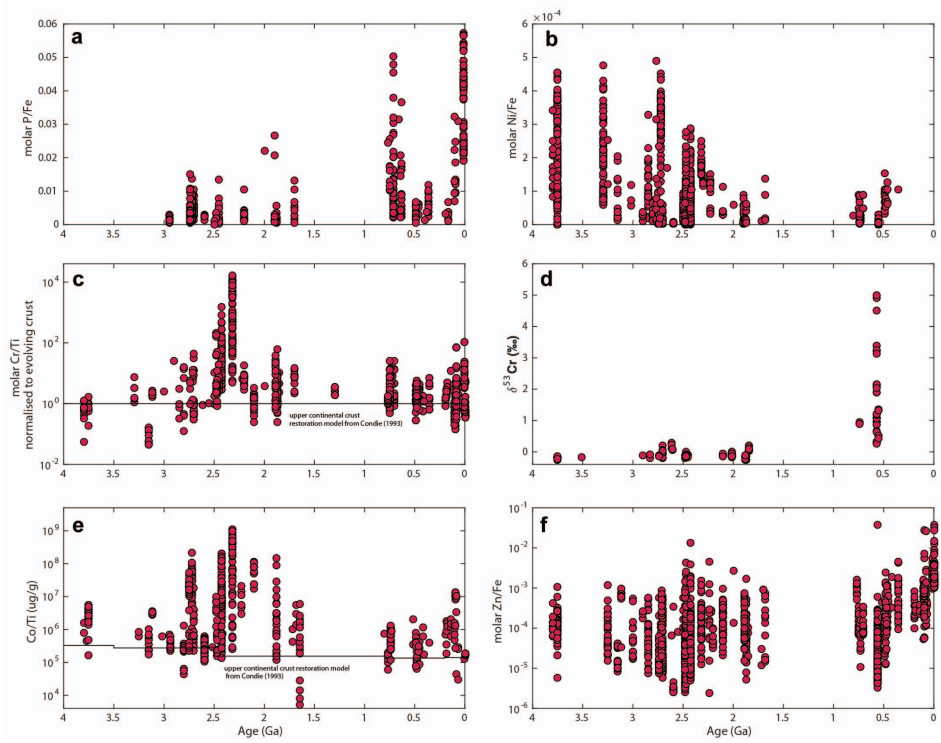

Figure 9. Several notable BIF trace element enrichment and isotope records: (a) phosphorus as molar P/Fe ratios from Planavsky *et al*. (2010b), (b) Ni as molar Ni/Fe ratios from Konhauser *et al*. (2015), (c) Cr as molar Cr/Ti ratios from Konhauser *et al*. (2011), (d) Cr isotope compositions from Frei et al. (2009), (e) Co as molar Co/Ti ratios from Swanner *et al*. (2015), and (f) Zn as molar Zn/Fe ratios from Robbins *et al*. (2013). See text for detailed explanations of each.

of pyrite on land produced significant acidity, which would have increased sulfate and nutrient fluxes to seawater (Reinhard *et al.*, 2009; Konhauser *et al.*, 2011; Bekker and Holland, 2012). This profound shift in weathering regimes constitutes Earth's first acid continental drainage system, and accounts for independent evidence of increased supply of sulfate (Bekker *et al.*, 2004) and sulfide-hosted trace elements to the oceans at that time (Scott *et al.*, 2008). With increased sulfate supply to the oceans, marine sulfate-reducing bacteria would have begun to dominate the anoxic layers of the water column, leading to the further marginalization of methanogens to the sulfate-poor bottom sediments, as is the case today. The end result of the progressive decline in methane production (a potent greenhouse gas) was a cooling climate, eventually culminating in the onset of major Palaeoproterozoic glaciations (Zahnle *et al.*, 2006).

During the past few years, Cr isotopes in BIF have also been used to track the progressive oxygenation of Earth's surface environment during the Archaean and Palaeoproterozoic (Fig. 9d). Frei *et al.* (2009) measured slight positive Cr

fractionations (+0.04 to +0.29 ‰) in samples deposited between 2.8 and 2.6 Ga, which they suggested was a first-order proxy for the presence of Cr(VI) in seawater at that time. Because of the efficient reduction of Cr(VI) by Fe^{2+} (which was abundant in the highly ferruginous Archaean oceans), and the near instantaneous precipitation of $(Fe,Cr)(OH)_3$ at seawater pH, the stable Cr isotope signatures of BIF should thus mirror the initial reaction of Cr(III) from mineral dissolution on land with MnO_2. Interestingly, BIF deposited between 2.5 and 1.9 Ga show minimal positive fractionations in Cr isotopes, suggesting that oxygen levels then dropped in the aftermath of the GOE. This is an unusual finding in that it was previously believed that atmospheric O_2 levels progressively increased post GOE (Kump, 2008), but the Cr isotope record in BIF instead documents transient fluctuations in atmospheric oxygenation. Most recently, Crowe *et al.* (2013) reported ^{53}Cr-depletion in 2.96 Ga palaeosols (ancient soil horizons) and ^{53}Cr-enrichment in overlying 2.96 Ga BIF. These near-contemporaneous units thus seem to have captured the Cr(VI) pool originating from oxidative continental weathering to chemical sedimentation some 500 Ma before the GOE. Based on the assumption that export of Cr(VI) from the weathering environment to the oceans necessitate minimal encounter with Fe(II) in rivers or groundwater, those authors further calculated that oxygen concentration were possibly as high as 3×10^{-4} present atmospheric levels.

Frei *et al.* (2009, 2012) reported further strong positive fractionations (δ^{53}Cr up to +4.9‰) in the late Neoproterozoic, suggestive of increased surface oxygenation at that time. Importantly, this work provided supporting evidence that linked a significant rise in global oxygenation to the emergence of early animals (*e.g.* Planavsky *et al.*, 2010b). If positive δ^{53}Cr are indicative of oxidative weathering, then the lack of such fractionations suggests minimal O_2 (to produce the MnO_2 catalyst). Indeed, in a recent study of granular Fe formations (reworked BIF) that were deposited between 1.7 and 0.9 Ga, Planavsky *et al.* (2014) observed δ^{53}Cr of −0.12‰. They hypothesized that the lack of Cr redox cycling must reflect atmospheric O_2 levels <0.1% present atmospheric levels, values below the theoretical estimates for the minimum O_2 requirements of the earliest animals. In other words, after the GOE oxygen levels plummeted, and it was not until the Neoproterozoic that O_2 levels increased sufficiently to facilitate animal evolution.

Cobalt is a bio-essential trace element and co-limiting (*e.g.* with Fe) nutrient in some regions of the modern oceans. It has been proposed that Co was more abundant in poorly ventilated Precambrian oceans based on the greater utilization of Co by anaerobic microbes relative to plants and animals. Based on the sedimentary record of Co enrichments and a model of marine Co sources and sinks (Fig. 9e), Swanner *et al.* (2014) proposed that before ~1.8 Ga the large volume of hydrothermal fluids circulating through abundant submarine ultramafic rocks and the predominance of anoxic sediments with a negligible capacity for Co burial resulted in a large marine Co reservoir. A decrease in marine Co concentrations in the Middle Proterozoic resulted from waning hydrothermal Co sources and the expansion of oxic and euxinic sediments that buried Co with Mn(III,IV) oxides or pyrite, respectively. It is interesting to note that the initial diversification of eukaryotes, and thus eukaryotic Co-utilizing genes,

occurred in the middle to late Proterozoic (*e.g.* Knoll *et al.*, 2007), at a time when marine Co concentrations were declining. Along similar lines, marine cyanobacteria likely utilize Co-binding ligands as a strategy for Co acquisition (Saito and Moffett, 2001; Saito *et al.*, 2005), which may help to explain their adaptation to low-Co environments despite high physiological demand. Perhaps this suggests that the number of Co-utilizing genes encoded by an organism's genome do not always mirror the metal's availability.

The lack of a clear link between metabolic metal demands and environmental concentrations is most clearly demonstrated by Zn. The relatively late proliferation of Zn metallomes by eukaryotes had previously been linked to marine Zn biolimitation (Williams and da Silva, 1996; Saito *et al.*, 2003; Dupont *et al.*, 2010). However, a recent examination of the BIF and shale records (Robbins *et al.*, 2013; Scott *et al.*, 2012, respectively; Fig. 9f) indicate that Zn may have been near modern abundances and was likely bioavailable to eukaryotes throughout the Precambrian, casting doubt on the coupled geochemical and eukaryotic evolutions with respect to Zn utilization. A novel possibility stemming from this work is that the late proliferation of Zn metalloenzymes in eukaryotes could have been a biologically intrinsic process related to the regulation of increasingly complex genomes, rather than solely dependent on the dramatic changes in the marine bioavailability of aqueous Zn species.

3.2. Ferromanganese crusts

Ferromanganese crusts have received significant attention due their ability to sorb certain trace elements from seawater, in particular Mo and Co. Molybdenum is supplied to the oceans primarily by the riverine flux of molybdate (MoO_4^{2-}) derived from the oxidative weathering of sulfide minerals (*e.g.* Archer and Vance, 2008). The molybdate anion is highly conservative, with a long residence time, in today's well mixed oceans. As a result, Mo is the most abundant transition element in the modern oxygenated oceans, at an average concentration of ~100 nM (Bertine and Turekian, 1973). The only significant sink for molybdate in well oxygenated environments is believed to be co-precipitation and burial with Mn oxyhydroxides, but this is a very slow process that removes only minor amounts of Mo from the ocean today (Bertine and Turekian, 1973). The adsorption of Co(II) and Co(III) to surface sites on ferric oxyhydroxides and Mn(III,IV) oxides, respectively, is an important pathway for scavenging of Co under oxic conditions (Koschinsky and Hein, 2003; Takahashi *et al.*, 2007; Stockdale *et al.*, 2010). By contrast, soluble Co maxima occur below the O_2-H_2S chemocline in modern euxinic basins in conjunction with both the soluble Fe and Mn peaks (Viollier *et al.*, 1995), which indicates that Co is released *via* the reductive dissolution of both Fe(III) oxyhydroxides and Mn(III,IV) oxides.

3.3. Black shales

3.3.1. Trace element concentrations

In modern sedimentary environments, black shales are used to examine palaeo-productivity based on trace element enrichments that correspond to increased organic

carbon burial (*e.g.* Tribovillard *et al.*, 2006) or the concentrations of trace elements relative to total organic carbon (Me/TOC) (*e.g.* Alego and Rowe, 2012). This linkage is mainly due to trace elements with multiple redox states being precipitated and enriched during periods of reducing conditions, *e.g.* uranium (U) and Mo under sulfidic conditions or Cr under ferruginous conditions (Arnold *et al.*, 2004; Dahl *et al.*, 2013; Partin *et al.*, 2013; Reinhard *et al.*, 2013) or incorporated into microbial biomass, *e.g.* Ni, Cu, Zn and Cd (Twining and Baines, 2013). Indeed, the utility of shales as palaeo-marine proxies has grown in recent years as an indicator of palaeo-environmental conditions on the ocean floor (*i.e.* oxic, ferruginous or euxinic) with the advent of Fe speciation analyses that assess the degree of pyritisation by comparing the ratio of pyrite Fe to reactive Fe (*e.g.* Raiswell and Canfield, 1998; Poulton and Canfield, 2005).

Black shales represent an important fraction of all ancient marine sediments preserved, and because of this, their trace element and isotope compositions have been used to track major biogeochemical events in Earth's history (*e.g.* Lyons *et al.*, 2009). This includes, amongst others: (1) the rise of atmospheric oxygen, (2) the onset of oxidative continental weathering, (3) the establishment of aerobic marine ecosystems, (4) the post-GOE drop in atmospheric O_2, and (5) the extent of Proterozoic marine euxinia. Arguably the smoking gun for the rise of atmospheric O_2 (*i.e.* the GOE) comes from the loss of sulfur isotope mass-independent fractionation (S-MIF) (Farquhar *et al.*, 2000). The processes that lead to S-MIF are restricted to the photochemical dissociation of SO_2 in the upper atmosphere into elemental and water-soluble S species. They then get rained out and incorporated into diagenetic pyrites, such as those associated with black shales. The only way to preserve the S-MIF signal is under low atmospheric O_2 levels because O_2 erases the unique signatures of these reactions and the presence of ozone prevents the penetration of ultraviolet radiation that generates the signals. The last appearance of S-MIF can be dated to pyrites in 2.32 Ga-old black shales of the Rooihoogte/Duitschland and Timeball Hills formations in South Africa, marking this point in Earth's history as a time of atmospheric oxygenation (Bekker *et al.*, 2004; Guo *et al.*, 2009).

In the past decade, several geochemical studies have been suggestive of oxidative continental weathering having occurred prior to the GOE. For example, increases in Mo and rhenium (Re) concentrations, as well as the first trend towards loss of S-MIF, comes from the 2.5 Ga Mount McRae Shale of Western Australia (Anbar *et al.*, 2007; Kaufman *et al.*, 2007). The trace element enrichments were interpreted as reflecting oxidative weathering of terrestrial sulfide minerals (but at much lower levels than at present), their transport to the oceans as dissolved oxyanion forms (*e.g.* MoO_4^{2-} and ReO_4^-), and then their being scavenged into black shales. The shales lack U enrichment, which, because it is predominantly hosted in silicates, would be less affected by rising atmospheric oxygen levels. Interestingly, Mo and Re enrichments were not observed in the upper sections of the shales, suggesting a subsequent drop in atmospheric O_2, or as coined by Anbar *et al.* (2007), the transient O_2 increase reflected a "whiff" of oxygen. Similar patterns of these metals had been reported in the 2.64–2.50 Ga Ghaap Group in South Africa (Wille *et al.*, 2007). Most recently, Stueken *et al.* (2012) suggested that an

increase in the total sulfur and Mo supply to marine shales at 2.8 Ga was best explained by the biological oxidation of crustal sulfide minerals.

Evidence in support of transient rises in atmospheric O_2 prior to the GOE implies the evolution and establishment of cyanobacteria in the ocean-water column. The presence of dissolved O_2 in seawater as early as 2.7 Ga is inferred from (i) black shales based on shifts toward heavier $\delta^{15}N$ values in kerogen consistent with the onset of an oxic nitrogen cycle (Godfrey and Falkowski, 2009), (ii) C isotope data in kerogens indicating methanotrophy (Eigenbrode and Freeman, 2006; Thomazo *et al.*, 2013), and (iii) coupled Fe and Mo isotopes that indicate the formation of ferric oxyhydroxides in the upper water column which were likely linked to cyanobacteria rather than photoferrotrophs (Czaja *et al.*, 2012): by 2.56 Ga, O_2 levels may have already reached several hundred metres on the continental slope (Kendall *et al.*, 2010). Based on the presence of 10 wt.% organic content in the 3.2 Ga Gorge Creek Group in north-western Australia, and the lack of Fe and sulfur, it is even possible that oxygenic photosynthesis may have evolved then. As Buick (2008) suggested, it is difficult to explain another mode of primary productivity that would have had enough available substrates over so wide an area for such lengths of time.

Until a few years ago, most researchers were of the opinion that once O_2 accumulated in the oceans and atmosphere it would have continued to rise until modern values were reached, sometime in the late Neoproterozoic (*e.g.* Kump, 2008). However, a study focusing on the temporal trends of U enrichment in black shale demonstrated that the initial rise of atmospheric O_2 at ~2.45 Ga was followed by a dramatic decline to less oxidizing conditions only several hundred million years after the GOE itself (Partin *et al.*, 2013). Somewhat similar trends were observed in the Mo and Mo/TOC records in black shales, but with evidence for a large oceanic Mo inventory occurring only at 2.2 Ga and then dropping to 10–20% of modern ocean levels until the Phanerozoic (Scott *et al.*, 2008). The smaller seawater Mo inventory, in the immediate aftermath of the GOE, was interpreted to reflect the Mo distribution in the continental crust, as has been argued for Re by Hannah *et al.* (2004). The present continental flux of Mo, like that of Re, is largely derived from organic matter-rich sulfidic shales; at the time of the GOE, the pre-GOE organic matter-rich sulfidic shales were not significantly enriched in Mo above crustal levels (Yamaguchi, 2002; Scott *et al.*, 2008). The predominant crustal reservoir of Mo that oxidized to form molybdate at this time would have been crystalline crustal rocks with generally low Mo content. This would result in a small supply of Mo to the oceans in the immediate aftermath of the GOE. The time for ingrowth of a large reservoir of Mo-enriched shales may have been comparable to the crustal residence time (200 Myr), and the process would ultimately lead to higher oceanic Mo contents as its concentration increased in the source rocks (*e.g.* black shales) that were being weathered.

The solubility and burial of U and Mo also depends on the sulfide concentration because both are chalcophilic. Therefore, in modern euxinic environments, such as the Black Sea, Mo sinks outpace Mo supply. Low Mo concentrations develop in the water column, and the magnitude of Mo enrichment and Mo/TOC ratios in sediments drop

precipitously (Algeo and Lyons 2006). This feature of Mo geochemistry forms the basis for the 'bio-inorganic bridge' hypothesis, whereby changes in the chemistry of the early oceans directly affected the bioavailability of trace elements, and in turn, the evolution of life (Anbar and Knoll, 2002). Those authors suggested that the drawdown of Mo under euxinic conditions limited primary photosynthetic productivity in the photic zone of the oceans for over a billion years between the late Palaeoproterozoic and Neoproterozoic (the so-called 'boring billion'; Buick *et al.*, 1995). The cause for the global euxinia was attributed to the progressive rise in atmospheric O_2 after the GOE that increased pyrite oxidation on land, which in turn led to a greater supply of dissolved sulfate to the oceans, enhanced sulfate reduction in the oceans, and the generation of sufficient dissolved sulfide that the total dissolved Fe flux in the oceans was titrated out by 1.8 Ga (Canfield, 1998). It was not until the Neoproterozoic, in association with a second large oxidation of the Earth's surface, that the deep oceans became oxygenated. However, the observed Mo drawdown and complementary Mo isotope data during that time interval are inconsistent with ocean-wide euxinia (*e.g.* Arnold *et al.*, 2004), and a recent investigation of sedimentary Mo and Cr enrichments in black shales, using mass-balance box models, demonstrated that only ~1–10% of the modern seafloor area needed to be anoxic at that time (Reinhard *et al.*, 2013).

3.3.2. Molybdenum isotopes in shales

When Mo removal from seawater is quantitative, the Mo isotope composition of reducing sediments may be directly linked to the isotopic composition of contemporaneous seawater, and in turn, to the relative importance of reducing and oxic areas of the seafloor. This property of the Mo isotope system has been extensively exploited to reconstruct palaeo-redox from black shales, whose organic-rich nature testify to depletion of available electron acceptors in the sedimentary pile and the establishment of reducing conditions (either anoxic or euxinic) amenable to recording the Mo isotope composition of contemporaneous seawater (section 2.4.2). Using a conservative assumption of 70% Mo removal by euxinic black shales in the mid-Proterozoic, Arnold *et al.* (2004) used simple isotope mass balance to calculate the Mo isotopic composition of mid-Proterozoic seawater to be around 0.8‰. This isotopically light value for seawater was interpreted to reflect expanded euxinia and a suppressed oxic sink. Assuming a riverine source near 0‰, Arnold *et al.* (2004) initially estimated a ratio between the fractional importance of oxic (f_{ox}) and euxinic (f_{eux}) sinks as being 10 times lower than today (f_{ox}/f_{eux} <0.4 in the mid-Proterozoic *vs.* ~3 today). Using a newly-determined modern riverine source value of ~0.7‰, Archer and Vance (2008) re-interpreted the low isotopic composition of mid-Proterozoic black shales (relative to modern seawater) as reflecting near total drawdown of the marine Mo reservoir as the result of expanded euxinia, with sedimentary Mo isotope compositions tending towards the source composition (mostly river water). In other words, Mo isotope data from shales reveal that mid-Proterozoic oceans were characterized by important euxinic Mo drawdown and little evidence for any important role for oxic sedimentary Mo exit channels. Similarly light (relative to modern seawater) Mo sedimentary isotope

compositions indicating near total absence of oxic Mo exit channels have been reported for black shales from the 2.05 Ga Palaeoproterozoic Shunga carbon burial event in the aftermath of the GOE (Asael *et al.*, 2013), during the mid-Neoproterozoic in the run-up to the appearance of the Ediacaran fauna (Dahl *et al.*, 2011), and during Phanerozoic ocean anoxic events (OAE) such as the Toarcian (early Jurassic) OAE (Pearce *et al.*, 2008). Using a mass-balance model with spatially variable metal burial rates and by also considering Cr (whose marine exit channels appear insensitive to the distinction between anoxia and euxinia), Reinhard *et al*. (2013) refined sedimentary Mo exit channels under low-O_2 (anoxic and euxinic) conditions, finding that a relatively small spatial extent of euxinia (1–10% of the seafloor, *vs.* 0.1% today) would be sufficient to crash the marine dissolved Mo reservoir, and by inference, draw seawater Mo isotope compositions towards riverine sources. Early models indicating widespread global euxinia throughout mid-Proterozoic oceans (*e.g.* Canfield *et al.*, 1998) are thus better characterized by expanded but spatially-restricted euxinia combined with widespread anoxia.

Molybdenum isotope-based redox proxies appear to be very sensitive to even the smallest amounts of free oxygen, and are now being used to examine trace amounts of dissolved Mo that may have been released prior to the ~2.4 Ga GOE and sustained oxidation of crustal Mo sources. Wille *et al.* (2007) demonstrated small but non-negligible Mo isotope deviations from crustal values in 2.6–2.5 Ga black shales from the Transvaal Supergroup, South Africa, indicating the production of some free O_2 at that time. In only slightly younger (2.50 Ga) black shales in the Hamersley basin, Western Australia, work by Anbar and colleagues (Anbar *et al.*, 2007; Duan *et al.*, 2010) has revealed coupled Mo abundance and isotope excursions occurring while the atmosphere remained anoxic, re-enforcing the idea that small, local oxygen-production events (*i.e.* "whiffs") likely preceded global oxygenation of the atmosphere. Kurzweil *et al.* (2015) extended the Hamersley Mo isotope dataset back by nearly 100 Ma to reveal a long-term trend of increasingly heavy Mo isotope compositions upwards in the basin. This would indicate a gradual increase in the prevalence of oxic Mo exit channels for seawater Mo prior to the GOE, consistent with the early occurrence of non-negligible Mo isotope fractionation as reported by Wille *et al.* (2007) for the contemporaneous Griqualand West basin, S. Africa.

4. Conclusions and future directions

By nature of their physicochemical surface properties, redox active Fe minerals are extremely efficient scavengers of trace elements from natural waters and so can be used to provide a rich archive of trace element concentrations and stable isotope compositions in terrestrial and marine environments over the entire history of their formation. These trace element signals can then be interpreted to shed light on environmental conditions in these environments at the time of mineral precipitation. Three Fe mineral archives are currently employed to help understand the evolution of Earth's redox and biogeochemical conditions, namely banded iron formations (BIF),

ferromanganese crusts and black shales, where although shales are not technically classed as Fe-rich sediments, it is likely that many of their trace elements are sequestered in association with Fe minerals. In these sediments Fe oxyhydroxides, including ferrihydrite, goethite, hematite and magnetite, and Fe sulfides, including pyrite, provide the primary Fe-rich phases for trace element sorption.

To date Fe mineral archives have provided a wealth of trace element concentration and stable isotope data which has been interpreted to reflect environmental conditions during Earth's earliest oceans and atmosphere, during the Archaean in the run up to and events after the Great Oxidation Event (GOE), through subsequent Ocean Anoxic Events (OAE), and into the relatively recent geological history of the Cenozoic. In light of these studies, it is certain that these enigmatic deposits have revolutionised our understanding of the Earth system. To continue forward with their investigation and bring new insights into Earth's redox and biogeochemical evolution, it is apparent that we must continue to improve our understanding of both the Fe mineral archives and the behaviour of their trace element impurities, both at the small-scale within the archives and at the larger-scale within the environment as a whole. By continuing to investigate the precipitation, deposition and diagenesis of Fe minerals, and both the macro- and microscopic uptake of trace elements to these minerals, we can be increasingly confident in the fidelity of trace element signals recorded in Fe mineral archives, and better able to relate these signals to the contemporaneous environment. Similarly, by continuing to investigate the role and function of trace elements in the environment, we can continue to make links between trace element signals recorded in Fe mineral archives and biogeochemical processes that reflect contemporaneous environmental conditions.

Acknowledgments

Financial support to CP from the Science and Technology Facilities Council (STFC) UK, and to KK from the Natural Sciences and Engineering Research Council of Canada (NSERC) is gratefully acknowledged.

References

Algeo, T.J. and Lyons, T.W. (2006) Mo-total organic carbon covariation in modern anoxic marine environments: Implications for analysis of paleoredox and paleo-hydrographic conditions. *Paleoceanography*, **21**, 1016, DOI: 10.1029/2004PA001112.

Algeo, T.J. and Rowe, H. (2012) Paleoceanographic applications of trace-metal concentration data. *Chemical Geology*, **324**, 6–18.

Alexander, B.W., Bau, M., Andersson, P. and Dulski, P. (2008) Continentally-derived solutes in shallow Archean seawater: Rare earth element and Nd isotope evidence in iron formation from the 2.9 Ga Pongola Supergroup, South Afric*a. Geochimica et Cosmochimica Acta*, **72**, 378–394.

Alexander, B.W., Bau, M. and Andersson, P. (2009) Neodymium isotopes in Archean seawater and implications for the marine Nd cycle in Earth's early oceans. *Earth and Planetary Science Letters*, **283**, 144–155.

Alibert, C. and McCulloch, M.T. (1993) Rare-earth element and neodymium isotopic compositions of the banded iron-formations and associated shales from Hamersley, Western-Australia. *Geochimica et Cosmochimica Acta*, **57**, 187–204.

Anbar, A.D. and Knoll, A.H. (2002) Proterozoic ocean chemistry and evolution: A bioinorganic bridge? *Science*, **297**, 1137.

Anbar, A.D., Roe, J.E., Barling, J. and Nealson, K.H. (2000) Nonbiological fractionation of iron isotopes. *Science*, **288**, 126–128.

Anbar, A.D., Jarzecki, A.A. and Spiro, T.G. (2005) Theoretical investigation of iron isotope fractionation between $Fe(H_2O)(^{3+})(_6)$ and $Fe(H_2O)(^{2+})(_6)$: Implications for iron stable isotope geochemistry. *Geochimica et Cosmochimica Acta*, **69**, 825–837.

Anbar, A.D., Duan Y., Lyons, T.W., Arnold, G.L., Kendall, B., Creaser, R.A., Kaufman, A.J., Gordon, G.W., Scott, C., Garvin, J. and Buick, R. (2007) A whiff of oxygen before the great oxidation event? *Science*, **317**, 1903–1906.

Archer, C. and Vance D. (2008) The isotopic signature of the global riverine molybdenum flux and anoxia in the ancient oceans. *Nature Geoscience*, **1**, 597–600.

Arnold, G.L., Anbar A.D., Barling J. and Lyons T.W. (2004) Molybdenum isotope evidence for widespread anoxia in mid-Proterozoic oceans. *Science*, **304**, 87–90.

Asael, D., Tissot, F.L.H., Reinhard, C.T., Rouxel, O., Dauphas, N., Lyons, T.W., Ponzevera, E., Liorzou, C. and Chéron, S. (2013) Coupled molybdenum, Fe and uranium stable isotopes as oceanic palaeo-redox proxies during the Palaeoproterozoic Shunga Event. *Chemical Geology*, **362**, 193–210.

Balci, N., Bullen, T., Witte-Lien, K., Shanks, W., Motelica, M. and Mandernack, K. (2006) Iron isotope fractionation during microbially stimulated Fe(II) oxidation and Fe(III) precipitation. *Geochimica et Cosmochimica Acta*, **70**, 622–639.

Barling, J. and Anbar, A.D. (2004) Molybdenum isotope fractionation during adsorption by manganese oxides. *Earth and Planetary Science Letters*, **217**, 315–329.

Barling,, J., Arnold, G.L. and Anbar, A.D. (2001) Natural mass-dependent variations in the isotopic composition of molybdenum. *Earth and Planetary Science Letters*, **193**, 447–457.

Balistrieri, L.S., Borrok, D.M., Wanty, R.B. and Ridley, W.I. (2008) Fractionation of Cu and Zn isotopes during adsorption onto amorphous Fe(III) oxyhydroxide: Experimental mixing of acid rock drainage and ambient river water. *Geochimica et Cosmochimica Acta*, **72**, 311–328.

Bau, M. and and Dulski, P. (1996) Distribution of yttrium and rare-earth elements in the Penge and Kuruman iron-formations, Transvaal Supergroup, South Afri*ca. Precambrian Research*, **79**, 37–55.

Bau, M., Hohndorf, A., Dulski, P. and Beukes, N.J. (1997) Sources of rare-earth elements and iron in paleoproterozoic iron-formations from the Transvaal Supergroup, South Africa: Evidence from neodymium isotopes. *Journal of Geology*, **105**, 121–129.

Beard, B., Johnson, C., Damm, von K. and Poulson, R. (2003) Iron isotope constraints on Fe cycling and mass balance in oxygenated Earth oceans. *Geology*, **31**, 629–632.

Bekker, A. and Holland, H.D. (2012) Oxygen overshoot and recovery during the early Paleoproterozoic. *Earth and Planetary Science Letters*, **317**, 295–304.

Bekker, A., Slack, J.F., Planavsky, N., Krapez, B., Hofmann, A., Konhauser, K.O. and Rouxel, O.J. (2010) Iron formation: The sedimentary product of a complex interplay among mantle, tectonic, oceanic, and biospheric processes. *Economic Geology*, **105**, 467–508.

Bekker, A., Holland, H.D., Wang, P.L., Rumble, D., Stein, H.J., Hannah, J.L., Coetzee L. L. and Beukes, N.J. (2004) Dating the rise of atmospheric oxygen. *Nature*, **427**, 117–120.

Belshaw, N.S., Zhu, X.K., Guo, Y. and O'Nions, R.K. (2000) High precision measurement of iron isotopes by plasma source mass spectrometry. *International Journal of Mass Spectrometry*, **197**, 191–195.

Berner, R.A. (1964) An idealized model of dissolved sulphate distribution in recent sediments. *Geochimica et Cosmochimica Acta*, **28**1497-1503.

Berner, R.A. (1981) A new geochemical classification of sedimentary environments. *Journal of Sedimentary Petrology*, **51**, 359–365.

Bertine, K.K. and Turekian, K.K. (1973) Molybdenum in marine deposits. *Geochimica et Cosmochimica Acta*, **37**, 1415–1434.

Bigeleisen, J. and Mayer, M.G. (1947) Calculation of equilibrium constants for isotopic exchange reactions. *Journal of Chemical Physics*, **15**, 261–267.

Bjerrum, C.J. and Canfield, D.E. (2002) Ocean productivity before about 1.9 Gyr ago limited by phosphorus

adsorption onto iron oxides. *Nature*, **417**, 159−162.
Boyd, P.W. and Ellwood, M.J. (2010) The biogeochemical cycle of iron in the ocean. *Nature Geoscience*, **3**, 675−682.
Boyle, E.A., Edmond, J.M. and Sholkovitz, E.R. (1977) The mechanism of iron removal in estuaries. *Geochimica et Cosmochimica Acta*, **41**, 1313−1324.
Braterman, P.S., Cairnssmith, A.G. and Sloper, R.W. (1983) Photooxidation of hydrated Fe2+ - Significance for banded iron formations. *Nature*, **303**, 163−164.
Brown, G.E. and Parks, G.A. (2001) Sorption of trace elements on mineral surfaces: Modern perspectives from spectroscopic studies, and comments on sorption in the marine environment. *International Geological Review*, **43**, 963−1073.
Buick, R. (2008) When did oxygenic photosynthesis evolve? *Philosophical Transactions of the Royal Society B*, **363**, 2731−2743.
Buick, R., Marais D.J.D. and Knoll, A.H. (1995) Stable isotope compositions of carbonates from the Mesoproterozoic Bangemall Group, northwestern Australia. *Chemical Geology*, **123**, 153−171.
Bullen, T.D., White, A.F., Childs, C.W. and Vivit, D.V. (2001) Demonstration of significant abiotic Fe isotope fractionation in nature. *Geology*, **29**, 699−702.
Burns, R.G. and Burns, V.M. (1977) Mineralogy of ferromanganese nodules. In *Marine Manganese Deposits* (G.P. Glasby, editor). Elsevier.
Byrne, R.H. and Sholkovitz, E.R. (1996) Marine chemistry and geochemistry of the lanthanides. Pp. 497−592 in: *Handbook on the Physics and Chemistry of Rare Earths*. Vol. **23** (K.A. Gschneider Jr. and L. Eyring, editors). Elsevier.
Canfield, D.E. (1998) A new model for Proterozoic ocean chemistry. *Nature*, **396**, 450−453.
Canfield, D.E., Thamdrup, B. and Hansen, J.W. (1993a) The anaerobic degradation of organic-matter in Danish coastal sediments – Iron reduction, manganese reduction and sulfate reduction. *Geochimica et Cosmochimica Acta*, **57**, 3867−3883.
Canfield, D.E., Jorgensen, B.B., Fossing, H., Glud, R., Gundersen, J., Ramsing, N.B., Thankdrup, B., Hansen, J.W., Nielsen, L.P. and Hall, P.O.J. (1993b) Pathways of organic-carbon oxidation in 3 continental-margin sediments. *Marine Geology*, **113**, 27−40.
Carazzo, G., Jellinek, A.M. and Turchyn, A.V. (2013) The remarkable longevity of submarine plumes: Implications for the hydrothermal input of iron to the deep-ocean. *Earth and Planetary Science Letters*, **382**, 66−76.
Cloud, P. (1973) Paleoecological significance of banded iron-formation. *Economic Geology*, **68**, 1135−1143.
Condie, K.C. (1993) Chemical composition and evolution of the upper continental crust - Contrasting results from surface samples and shales. *Chemical Geology*, **104**, 1−37.
Corliss, J.B., Lyle, M., Dymond, J. and Crane, K. (1978) Chemistry of hydrothermal mounds near Galapagos Rift. *Earth and Planetary Science Letters*, **40**, 12−24.
Cornell, R.M. and Schwertmann, U. (2003) *The Iron Oxides: Structure, Properties, Reactions, Occurrences and Uses, Second Edition*, Wiley-VCH Verlag GmbH and Co. KGaA, Weinheim.
Criss, R.E. (1999) *Principles of Stable Isotope Distribution*. Oxford University Press, Oxfprd, UK.
Croal, L., Johnson, C., Beard, B. and Newman, D. (2004) Iron isotope fractionation by Fe (II)-oxidizing photoautotrophic bacteria 1. *Geochimica et Cosmochimica Acta*, **68**, 1227−1242.
Crowe, S.A., Dossing, L.N., Beukes, N.J., Bau, M., Kruger, S.J., Frei, R. and Canfield, D.E. (2013) Atmospheric oxygenation three billion years ago. *Nature*, **501**, 535.
Czaja, A.D., Johnson, C.M., Beard, B.L., Roden, E.E., Li, W.Q. and Moorbath, S. (2013) Biological Fe oxidation controlled deposition of banded iron formation in the *ca.* 3770 Ma Isua Supracrustal Belt (West Greenland). *Earth and Planetary Science Letters*, **363**, 192−203.
Dahl, T.W., Canfield, D.E., Rosing, M.T., Frei, R.E., Gordon, G.W., Knoll, A.H. and Anbar, A.D. (2011) Molybdenum evidence for expansive sulfidic water masses in ~750 Ma oceans. *Earth and Planetary Science Letters*, **311**, 264−274.
Dahl, T.W., Chappaz, A., Fitts, J.P. and Lyons, T.W. (2013) Molybdenum reduction in a sulfidic lake: Evidence from X-ray absorption fine-structure spectroscopy and implications for the Mo paleoproxy. *Geochimica et Cosmochimica Acta*, **103**, 213−231.

Dauphas, N., Cates, N.L., Mojzsis, S.J. and Busigny, V. (2007) Identification of chemical sedimentary protoliths using Fe isotopes in the >3750 Ma Nuvvuagittuq supracrustal belt, Canada. *Earth and Planetary Science Letters*, **254**, 358–376.

Davis, J.A. and Leckie, J.O. (1978) Surface ionization and complexation at the oxide/water interface. II. Surface properties of amorphous Fe oxyhydroxide and adsorption of metal ions. *Journal of Colloid and Interface Science*, **67**, 90–105.

Dean, W.E. and Greeson, P.E. (1979) Influences of algae on the formation of freshwater ferromanganese nodules, Onedia Lake, New-York. *Archiv für Hydrobiologie*, **86**, 181–192.

Derry, L.A. and Jacobsen, S.B. (1988) The Nd and Sr isotopic evolution of Proterozoic seawater. *Geophysical Research Letters*, **15**, 397–400.

Derry, L.A. and Jacobsen, S.B. (1990) The chemical evolution of Precambrian seawater - Evidence from REEs in banded iron formations. *Geochimica et Cosmochimica Acta*, **54**, 2965–2977.

Duan, Y., Anbar, A.D., Arnold, G.L., Lyons, T.W., Gordon, G.W. and Kendall, B. (2010) Molybdenum isotope evidence for mild environmental oxygenation before the Great Oxidation Event. *Geochimica et Cosmochimica Acta*, **74**, 6655–6668.

Dupont, C.L., Butcher, A., Valas, R.E., Bourne, P.E. and Caetano-Anolles, G. (2010) History of biological metal utilization inferred through phylogenomic analysis of protein structures. *Proceedings of the National Academy of Sciences USA*, **107**, 10567–10572.

Dzombak, D.A. and Morel, F.M. (1990) *Surface Complexation Modelling: Hydrous Ferric Oxide.* Wiley-Interscience, New York.

Eary, L.E. and Rai, D. (1987) Kinetics of chromium(III) oxidation to chromium(VI) by reaction with manganese-dioxide. *Environmental Science and Technology*, **21**, 1187–1193.

Eary, L.E. and Rai, D. (1989) Kinetics of chromate reduction by ferrous-ions derived from hematite and biotite at 25-degrees-C. *American Journal of Science*, **289**, 180–213.

Edmonds, H.N. and German, C.R. (2004) Particle geochemistry in the Rainbow hydrothermal plume, Mid-Atlantic Ridge. *Geochimica et Cosmochimica Acta*, **68**, 759–772.

Eigenbrode, J.L. and Freeman, K.H. (2006) Late Archean rise of aerobic microbial ecosystems. *Proceedings of the National Academy of Sciences USA*, **103**, 15759–15764.

Ellis, A.S., Johnson, T.M. and Bullen, T.D. (2002) Chromium isotopes and the fate of hexavalent chromium in the environment. *Science*, **295**, 2060–2062.

Ellis, A.S., Johnson, T.M. and Bullen, T.D. (2004) Using chromium stable isotope ratios to quantify Cr(VI) reduction: Lack of sorption effects. *Environmental Science and Technology*, **38**, 3604–3607.

Erickson, B.E. and Helz G.R. (2000) Molybdenum(VI) speciation in sulfidic waters: Stability and lability of thiomolybdates. *Geochimica et Cosmochimica Acta*, **64**, 1149–1158.

Farquhar, J., Bao, H.M. and Thiemens, M. (2000) Atmospheric influence of Earth's earliest sulfur cycle. *Science*, **289**, 756–758.

Feely, R.A., Massoth, G.J., Baker, E.T., Cowen, J.P., Lamb, M.F. and Krogslund, K.A. (1990) The effect of hydrothermal processes on midwater phosphorus distributions in the northeast Pacific. *Earth and Planetary Science Letters*, **96**, 305–318.

Feely, R.A., Trefry, J.H., Lebon, G.T. and German, C.R. (1998) The relationship between P/Fe and V/Fe ratios in hydrothermal precipitates and dissolved phosphate in seawater. *Geophysical Research Letters*, **25**, 2253–2256.

Fendorf, S. (1995) Surface-reactions of chromium in soils and waters. *Geoderma* 67, 55–71.

Fischer, W.W. and Knoll, A.H. (2009) An iron shuttle for deepwater silica in Late Archean and early Proterozoic iron formation. *Geological Society of America Bulletin*, **121**, 222–235.

Frei, R. and Polat, A. (2007) Source heterogeneity for the major components of similar to 3.7 Ga Banded Iron Formations (Isua Greenstone Belt, Western Greenland): Tracing the nature of interacting water masses in BIF formation. *Earth and Planetary Science Letters*, **253**, 266–281.

Frei, R., Dahl, P.S., Duke, E.F., Frie, K.M., Hansen, T.R., Frandsson, M.M. and Jensen, L.A. (2008) Trace element and isotopic characterization of Neoarchean and Paleoproterozoic iron formations in the Black Hills (South Dakota, USA): Assessment of chemical change during 2.9–1.9 Ga deposition bracketing the 2.4–2.2 Ga first rise of atmospheric oxygen. *Precambrian Research*, **162**, 441–474.

Frei, R., Gaucher, C., Poulton, S.W. and Canfield, D.E. (2009) Fluctuations in Precambrian atmospheric oxygenation recorded by chromium isotopes. *Nature*, **461**, 250–253.

Frierdich, A.J., Luo, Y. and Catalano, J.G. (2011) Trace element cycling through iron oxide minerals during redox-driven dynamic recrystallization. *Geology*, **39**, 1083–1086.

Frost, C., Blanckenburg, F. von, Schoenberg, R., Frost B. and Swapp, S. (2007) Preservation of Fe isotope heterogeneities during diagenesis and metamorphism of banded Fe formation. *Contributions to Mineralogy and Petrology*, **153**, 211–235.

Gallagher, M., Turner, E.C. and Kamber, B.S. (2015) *In situ* trace element analysis of Neoarchean - Ordovician shallow-marine microbial-carbonate-hosted pytires. *Geobiology*, doi: 10.1111/gbi.12139.

Garrels, R.M., Perry, E.A. and Mackenzi, F.T. (1973) Genesis of Precambrian iron-formations and development of atmospheric oxygen. *Economic Geology*, **68**, 1173–1179.

German, C.R. and Elderfield, H. (1990) Rare-earth elements in the NW Indian-Ocean. *Geochimica et Cosmochimica Acta*, **54**, 1929–1940.

German, C.R., Holliday, B.P. and Elderfield, H. (1991) Redox cycling of rare-earth elements in the suboxic zone of the Black Sea. *Geochimica et Cosmochimica Acta*, **55**, 3553–3558.

Glasby, G.P. (1977) *Marine Manganese Deposits*. Elsevier.

Godfrey, L.V. and Falkowski, P.G. (2009) The cycling and redox state of nitrogen in the Archean ocean. *Nature Geoscience*, **2**, 725–729.

Goldberg, T., Archer, C., Vance, D. and Poulton, S.W. (2009) Mo isotope fractionation during adsorption to Fe (oxyhydr)oxides. *Geochimica et Cosmochimica Acta*, **73**, 6502–6516.

Goldberg, T., Archer, C., Vance, D., Thamdrup, B., McAnena, A. and Poulton, S.W. (2012) Controls on Mo isotope fractionations in a Mn-rich anoxic marine sediment, Gullmar Fjord, Sweden. *Chemical Geology*, **296–297**, 73–82.

Goldberg, T., Gordon, G., Izon, G., Archer, C., Pearce, C.R., Mcmanus, J., Anbar, A.D. and Rehkamper, M. (2013) Resolution of inter-laboratory discrepancies in Mo isotope data: an intercalibration. *Journal of Analytical and Atomic Spectroscopy*, **28**, 724–735.

Greber, N.D., Siebert, C., Nägler, T.F. and Pettke, T. (2012) $\delta^{98/95}$Mo values and Molybdenum Concentration Data for NIST SRM 610, 612 and 3134: Towards a Common Protocol for Reporting Mo Data. *Geostandards and Geoanalytical Research*, **36**, 291–300.

Grenne, T. and Slack, J.F. (2003) Paleozoic and Mesozoic silica-rich seawater: Evidence from hematitic chert (jasper) deposits. *Geology*, **31**, 319–322.

Grotzinger, J.P. (1990) Geochemical model for Proterozoic stromatolite decline. *American Journal of Science*, **290A**, 80–103.

Grotzinger, J.P. and Knoll, A.H. (1999) Stromatolites in Precambrian carbonates: Evolutionary mileposts or environmental dipsticks? *Annual Reviews in Earth and Planetary Science*, **27**, 313–358.

Guo, Q.J., Strauss, H., Kaufmann, A.J., Schroder, S., Gutzmer, J., Wing, B., Baker, M.A., Bekker, A., Jin, Q.S., Kim, S.T. and Farquhar, J. (2009) Reconstructing Earth's surface oxidation across the Archean-Proterozoic transition. *Geology*, **37**, 399–402.

Haese, R.R. (2000) The reactivity of iron. Pp. 233–261 in: *Marine Geochemistry.* Springer Berlin, Heidelberg, Berlin.

Hannah, J.L., Bekker, A., Stein, H.J., Markey, R.J. and Holland, H.D. (2004) Primitive Os and 2316 Ma age for marine shale: implications for Paleoproterozoic glacial events and the rise of atmospheric oxygen. *Earth and Planetary Science Letters*, **225**, 43–52.

Hartman, H. (1984) The evolution of photosynthesis and microbial mats: A speculation on the banded iron formations. Pp. 449–454 in: *Microbial Mats: Stromatolites* (Y. Cohen, R.W. Castenholz and H.O. Halvorson, editors). Alan R. Liss, Inc. New York.

Haugaard, R., Frei, R., Stendal, H. and Konhauser, K.O. (2013) Petrology and geochemistry of the similar to 2.9 Ga Itilliarsuk banded iron formation and associated supracrustal rocks, West Greenland: Source characteristics and depositional environment. *Precambrian Research*, **229**, 150–176.

Hein, J.R., Yeh, H.W., Gunn, S.H., Sliter, W.V., Benninger, L.m. and Wang, C.H. (1993) Two major episodes of phosphogenesis recorded in equatorial Pacific seamount deposits. *Paleoceanography*, **8**, 293–311.

Hein, J.R., Koschinsky, A., Bau, M., Manheim, F.T., Kang, J.-K. and Roberts, L. (2000) Cobalt-rich

ferromanganese crusts in the Pacific. Pp. 239–279 in: *Handbook of Marine Mineral Deposits* (D.S. Cronan, editor). CRC Press, Boca Raton, Florida, USA.

Hein, J.R., Mizell, K., Koschinsky, A. and Conrad, T.A. (2013) Deep-ocean mineral deposits as a source of critical metals for high- and green-technology applications: Comparison with land-based resources. *Ore Geology Review*, **51**, 1–14.

Helz, G.R., Miller, C.V., Charnock, J.M., Mosselmans, J.F.W., Pattrick, R.A.D., Garner, C.D. and Vaughan, D.J. (1996) Mechanism of molybdenum removal from the sea and its concentration in black shales: EXAFS evidence. *Geochimica et Cosmochimica Acta*, **60**, 3631–3642.

Hill, P.S. and Schauble, E.A. (2008) Modeling the effects of bond environment on Fe isotope fractionation in ferric aquo-chloro complexes. *Geochimica et Cosmochimica Acta*, **72**, 1939–1958.

Holland, H.D. (1973) Oceans – Possible source of iron in iron-formations. *Economic Geology*, **68**, 1169–1172.

Holland, H.D. (1984) *The Chemical Evolution of the Atmosphere and Oceans*. Princeton Univ. Press, Princeton.

Holm, N.G. (1989) The C-13 C-12 ratios of siderite and organic-matter of a modern metalliferous hydrothermal sediment and their implications for banded iron formations. *Chemical Geology*, **77**, 41–45.

Huerta-Diaz, M.A. and Morse, J.W. (1992) Pyritization of trace elements in anoxic marine sediments. *Geochimica et Cosmochimica Acta*, **56**, 2681–2702.

Huston, D.L. and Logan, G.A. (2004) Barite, BIFs and bugs: Evidence for the evolution of the Earth's early hydrosphere. *Earth and Planetary Science Letters*, **220**, 41–55.

Ihler, R.K. (1979) *Chemistry of Silica*. Wiley-Interscience, New York

Jacobsen, S.B. and Pimentel-Klose, M.R. (1988) Nd isotopic variations in Precambrian banded iron formations. *Geophysical Research Letters*, **15**, 393–396.

James, H.L. (1954) Sedimentary facies of iron formations. *Economic Geology*, **49**, 235–293.

Jickells, T.D., An, Z.S., Andersen, K.K., Baker, A.R., Bergametti, G., Brooks, N., Cao, J.J., Boyd, P.W., Duce, R.A., Hunter, K.A., Kawahata, H., Kubilay, N., laRoche, J., Liss, P.S., Mahowald, N., Prospero, J.M., Ridgwell, A.J., Tegen, I. and Torres, R. (2005) Global iron connections between desert dust, ocean biogeochemistry, and climate. *Science*, **308**, 67–71.

Johnson, C.M., Skulan, J.L., Beard, B.L., Sun, H., Nealson, K.H. and Braterman, P.S. (2002) Isotopic fractionation between Fe(III) and Fe(II) in aqueous solutions. *Earth and Planetary Science Letters*, **195**, 141–153.

Johnson, C.M., Beard, B.L., Beukes, N.J., Klein, C. and O'Leary, J.M. (2003) Ancient geochemical cycling in the Earth as inferred from Fe isotope studies of banded iron formations from the Transvaal Craton. *Contributions to Mineralogy and Petrology*, **144**, 523–547.

Johnson, C.M., Beard, B.L. and Albarede, F. (2004) Overview and general concepts. Pp. 1–24 in: *Geochemistry of Non-Traditional Stable Isotopes* (C.M. Johnson, B.L. Beard and F. Albarede, editors). Reviews in Mineralogy and Geochemistry, **55**. Mineralogical Society of America and the Geochemical Society, Washington, D.C.

Johnson, C.M., Beard, B.L., Klein, C., Beukes, N.J. and Roden, E.E. (2008a) Iron isotopes constrain biologic and abiologic processes in banded Fe formation genesis. *Geochimica et Cosmochimica Acta*, **72**, 151–169.

Johnson, C.M., Beard, B.L. and Roden, E.E. (2008b) The iron isotope fingerprints of redox and biogeochemical cycling in modern and ancient Earth. *Annual Reviews in Earth and Planetary Science*, **36**, 457–493.

Jones, C., Nomosatryo, S., Crowe, S.A., Bjerrum, C.J. and Canfield, D.E. (2015) Iron oxides, divalent cations, silica, and the early Earth phosphorus crisis. *Geology*, **43**, 135–138.

Kappler, A., Pasquero, C., Konhauser, K.O. and Newman, D.K. (2005) Deposition of banded iron formations by anoxygenic phototrophic Fe(II)-oxidising bacteria. *Geology*, **33**, 865–868.

Kashiwabara, T., Takahashi Y. and Tanimizu, M. (2011) Molecular-scale mechanisms of distribution and isotopic fractionation of molybdenum between seawater and ferromanganese oxides. *Geochimica et Cosmochimica Acta*, **75**, 5762–5784.

Kaufman, A.J., Johnston, D.T., Farquhar, J., Masterson, A.L., Lyons, T.W., Bates, S., Anbar, A.D., Arnold, G.L., Garvin, J. and Buick, R. (2007) Later Archean biospheric oxygenation and atmospheric evolution. *Science*, **317**, 1900–1903.

Kendall, B., Reinhart, C.T., Lyons, T., Kaufman, A.J., Poulton, S.W. and Anbar, A.D. (2010) Pervasive oxygenation along late Archean ocean margins. *Nature Geoscience*, **3**, 647–652.

Kennedy, C.B., Martinez, R.E., Scott, S.D. and Ferris, F.G. (2003) Surface chemistry and reactivity of bacteriogenic iron oxides from Axial Volcano, Juan de Fuca Ridge, north-east Pacific Ocean. *Geobiology*, **1**, 59–69.

Klein, C. (2005) Some Precambrian banded iron-formations (BIFs) from around the world: Their age, geologic setting, mineralogy, metamorphism, geochemistry, and origin. *American Mineralogist*, **90**, 1473–1499.

Klein, C. and Beukes, N.J. (1989) Geochemistry and sedimentology of a facies transition from limestone to iron-formation deposition in the early Proterozoic Transvaal Supergroup, South-Africa. *Economic Geology*, **84**, 1733–1774.

Klein, C., and Beukes, N.J., 1992. Time distribution, stratigraphy, and sedimentologic setting, and geochemistry of Precambrian iron-formations. Pp. 139–146 in: *The Proterozoic Biosphere: A Multidisciplinary Study* (J.W. Schopf, and C. Klein, editors). Cambridge University Press. Cambridge, UK.

Klinkhammer, G., Elderfield, H. and Hudson, A. (1983) Rare-earth elements in seawater near hydrothermal vents. *Nature*, **305**, 185–188.

Knoll, A.H., Summons, R.E., Waldbauer, J.R. and Zumberge, J.E. (2007) The geological succession of primary producers in the oceans. Pp. 133–163 in: *Evolution of Primary Producers in the Sea* (P.G. Falkowski and A.H. Knoll, editors). Elsevier, Amsterdam.

Konhauser, K., Hamade, T., Raiswell, R., Morris, R.C., Ferris, F.G., Southam, G. and Canfield, D.E. (2002) Could bacteria have formed the Precambrian banded iron formations? *Geology*, **30**, 1079–1082.

Konhauser, K.O., Newman, D.K. and Kappler, A. (2005) The potential significance of microbial Fe(III) reduction during deposition of Precambrian banded iron formations. *Geobiology*, **3**, 167–177.

Konhauser, K.O., Lalonde, S.V., Amskold L. and Holland, H.D. (2007) Was there really an Archean phosphate crisis? *Science*, **315**, 1234.

Konhauser, K.O., Pecoits, E., Lalonde, S.V., Papineau, D., Nisbet, E.G., Barley, M.E., Arndt, N.T., Zahnle, K. and Kamber, B.S. (2009) Oceanic Ni depletion and a methanogen famine before the great oxidation event. *Nature*, **458**, 750–753.

Konhauser, K.O., Lalonde, S.V., Planavsky, N.J., Pecoits, E., Lyons, T.W., Mojzsis, S.J., Rouxel, O.J., Barley, M.E., Rosiere, C., Fralick, P.W., Kump, L.R. and Bekker, A. (2011) Aerobic bacterial pyrite oxidation and acid rock drainage during the Great Oxidation Event. *Nature*, **478**, 369.

Konhauser, K.O., Robbins L.J., Pecoits, E., Peacock, C., Kappler, A. and Lalonde, S.V. (2015) The Archean nickel famine revisited. *Astrobiology*, **15**, 804–815.

Koschinsky, A. and Halbach, P. (1995) Sequential leaching of marine ferromanganese precipitates: Genetic implications. *Geochimica et Cosmochimica Acta*, **59**, 5113–5132.

Koschinsky, A. and Hein, J.R. (2003) Uptake of elements from seawater by ferromanganese crusts: Solid-phase associations and seawater speciation. *Marine Geology*, **198**, 331–351.

Koschinsky, A., Stascheit, A., Bau, M. and Halbach, P. (1997) Effects of phosphatization on the geochemical and mineralogical composition of marine ferromanganese crusts. *Geochimica et Cosmochimica Acta*, **61**, 4079–4094.

Kump, L.R. (2008) The rise of atmospheric oxygen. *Nature*, **451**, 277–278.

Kurzweil, F., Wille, M., Schoenberg, R., Taubald, H. and Van Kranendonk, M.J. (2015) Continuously increasing δ^{98}Mo values in Neoarchean black shales and iron formations from the Hamersley Basin. *Geochimica et Cosmochimica Acta*, **164**, 523–542.

Lalonde, S., Konhauser, K.O., Amskold, L., McDermott, T. and Inskeep, B.P. (2007) Chemical reactivity of microbe and mineral surfaces in hydrous ferric oxide depositing hydrothermal springs. *Geobiology*, **5**, 219–234.

Langmuir, D. (1997) *Aqueous Environmental Geochemistry*. Prentice Hall, New Jersey.

Large, R.R., Danyushevsky, L., Hollit, C., Maslennikov, V., Meffre, S., Gilbert, S., Bull, S., Scott, R., Emsbo, P., Thomas, H., Singh, B. and Foster, J. (2009) Gold and trace element zonation in pyrite using a laser imaging technique: Implications for the timing of gold in orogenic and carlin-style sediment-hosted deposits. *Economic Geology*, **104**, 635–668.

Large, R.R., Halpin, J.A., Danyushevsky, L.V., Maslennikov, V.V., Bull, S.W., Long, J.A., Gregory, D.D., Lounejeva, E., Lyons, T.W., Sack, P.J., McGoldrick, P.J . and Claver, C.R. (2014) Trace element content of sedimentary pyrite as a new proxy for deep-time ocean-atmosphere evolution. *Earth and Planetary Science*

Letters, **389**, 209–220.
Ler, A. and Stanforth, R. (2003) Evidence for surface precipitation of phosphate on goethite. *Environmental Science & Technology*, **37**, 2694–2700.
Lepp, H. and Goldich, S.S. (1964) Origin of Precambrian iron formations. *Economic Geology*, **59**, 1025–1061.
Lindemann, F.A. (1919) Note on the vapour pressure and affinity of isotopes. *Philosophical Magazine*, **38**, 173–181.
Lindemann, F.A. and Aston, F.W. (1919) The possibility of separating isotopes. *Philosophical Magazine*, **37**, 530.
Little, S.H., Sherman, D.M., Vance, D. and Hein, J.R. (2014) Molecular controls on Cu and Zn isotope fractionation in Fe-Mn crusts. *Earth and Planetary Science Letters*, **396**, 213–222.
Lyons, T.W., Anbar, A.D., Severmann, S., Scott, C. and Gill, B.C. (2009) Tracking euxinia in the ancient ocean: A multiproxy perspective and Proterozoic case study. *Annual Reviews in Earth and Planetary Science*, **37**, 507–534.
Mackenzie, F.T., Lantzy, R.J. and Paterson, V. (1979) Global trace element cycles and predictions. *Mathematical Geology*, **11**, 99–142.
Maliva, R.G., Knoll, A.H. and Simonson, B.M. (2005) Secular change in the Precambrian silica cycle: insights from chert petrology. *Geological Society of America Bulletin*, **117**, 835–845.
Manceau, A. and Charlet, L. (1992) X-ray absorption spectroscopic study of the sorption of Cr(III) at the oxide water interface. 1. Molecular mechanism of Cr(III) oxidation on Mn oxides. *Journal of Colloid and Interface Science*, **148**, 425–442.
McNamara, K.J. and Awramik, S.M. (1992) Stromatolites – A key to understanding the early evolution of life. *Science Progress*, **76**, 345–364.
McManus, J., Nagler, T.F., Siebert, C., Wheat, C.G. and Hammond, D.E. (2002) Oceanic molybdenum isotope fractionation: Diagenesis and hydrothermal ridge-flank alteration. *Geochemistry Geophysics Geosystems*, **3**, 1078.
Mero, J.L. (1962) Ocean floor manganese nodules. *Economic Geology*, **57**, 747–767.
Miller, R.G. and O'Nions, R.K. (1985) Source of Precambrian chemical and clastic sediments. *Nature*, **314**, 325–330.
Moon, E.M. and Peacock, C.L. (2011) Adsorption of Cu(II) to Bacillus subtilis: A pH-dependent EXAFS and thermodynamic modelling study. *Geochimica et Cosmochimica Acta*, **75**, 6705–6719.
Moon, E.M. and Peacock, C.L. (2012) Adsorption of Cu(II) to ferrihydrite and ferrihydrite-bacteria composites: Importance of the carboxyl group for Cu mobility in natural environments. *Geochimica et Cosmochimica Acta*, **92**, 203–219.
Moon, E.M. and Peacock, C.L. (2013) Modelling Cu(II) adsorption to ferrihydrite and ferrihydrite-bacteria composites: Deviation form additive adsorption in the composite sorption system. *Geochimica et Cosmochimica Acta*, **104**, 148–164.
Morris, R.C. (1993) Genetic modelling for banded iron-formation of the Hamersley Group, Pilbara Craton, Western Australia. *Precambrian Research*, **60**, 243–286.
Morse, J.W. and Arakaki, T. (1993) Adsorption and coprecipitation of divalent metals with mackinawite (FeS). *Geochimica et Cosmochimica Acta*, **57**, 3635–3640.
Morse, J.W. and Luther, G.W. (1999) Chemical influences on trace element-sulfide interactions in anoxic sediments. *Geochimica et Cosmochimica Acta*, **63**, 3373–3378.
Muios, S.B., Hein, J.R., Frank, M., Monteiro, J.H., Gaspar, L., Conrad, T., Pereira, H.G. and Abrantes, F. (2013) Deep-sea Fe-Mn crusts from the Northeast Atlantic Ocean: Composition and resource considerations. *Marine Georesources and Geotechnology*, **31**, 40–70.
Nakada, R., Takahashi, Y. and Tanimizu, M. (2013) Isotopic and speciation study on cerium during its solid-water distribution with implication for Ce stable isotope as a palaeo-redox proxy. *Geochimica et Cosmochimica Acta*, **103**, 49–62.
Nielsen, S.G., Wasylenki, L.E., Rehkamper, M., Peacock, C.L., Xue, Z.C. and Moon, E.M. (2013) Towards and understanding of thallium isotope fractionation during adsorption to manganese oxides. *Geochimica et Cosmochimica Acta*, **117**, 252–265.
O'Neil, J.R. (1986) Theoretical and experimental aspects of isotopic fractionation. Pp. 1–40 in: *Stable Isotopes*

in High Temperature Geological Processes (J.W. Valley, H.P. Taylor and J.R. O'Neil, editors). Reviews in Mineralogy, **16**. Mineralogical Society of America, Washington, D.C.

Partin, C.A., Bekker, A., Planavsky, N.J., Scott, C.T., Gill, B.C., Li, C., Podkovyrov, V., Maslov, A., Konhauser, K.O., Lalonde, S.V., Love, G.D., Poulton, S.W. and Lyons, T.W. (2013) Large-scale fluctuations in Precambrian atmospheric and oceanic oxygen levels from the record of U in shales. *Earth and Planetary Science Letters*, **369**, 284–293.

Peacock, C.L. (2009) Physiochemical controls on the crystal-chemistry of Ni in birnessite: Genetic implications for ferromanganese precipitates. *Geochimica et Cosmochimica Acta*, **73**, 3568–3578.

Peacock, C.L. and Moon, E.M. (2012) Oxidative scavenging of thallium by birnessite: Explanation for thallium enrichment and stable isotope fractionation in marine ferromanganese precipitates. *Geochimica et Cosmochimica Acta*, **84**, 297–313.

Peacock, C.L. and Sherman, D.M. (2004a) Vanadium adsorption onto goethite (a-FeOOH) at pH 1.5 to 12: A surface complexation model based on ab inito molecular geometries and EXAFS spectroscopy. *Geochimica et Cosmochimica Acta*, **68**, 1723–1733.

Peacock, C.L. and Sherman, D.M. (2004b) Copper (II) sorption onto goethite, hematite and lepidocrocite: A surface complexation model based on ab inito molecular geometries and EXAFS spectroscopy. *Geochimica et Cosmochimica Acta*, **68**, 2623–2637.

Peacock, C.L. and Sherman, D.M. (2007) Sorption of Ni by birnessite: equilibrium controls on Ni in seawater. *Chemical Geology*, **238**, 94-106.

Pearce, C.R., Cohen, A.S., Coe, A.L. and Burton, K.W. (2008) Molybdenum isotope evidence for global ocean anoxia coupled with perturbations to the carbon cycle during the Early Jurassic. *Geology*, **36**, 231–234.

Pecoits, E., Smith, M.L., Catling, D.C., Philippot, P., Kappler A. and Konhauser, K.O. (2015) Atmospheric hydrogen peroxide and Eoarchean iron formations. *Geobiology*, **13**, 1–14.

Pea, J., Kwon, K.D., Refson, K., Bargar, J.R. and Sposito, G. (2010) Mechanisms of nickel sorption by a bacteriogenic birnessite. *Geochimica et Cosmochimica Acta*, **74**, 3076–3089.

Planavsky, N., Rouxel, O., Bekker, A., Shapiro, R., Fralick, P. and Knudsen, A. (2009) Iron-oxidizing microbial ecosystems thrived in late Paleoproterozoic redox-stratified oceans. *Earth and Planetary Science Letters*, **286**, 230–242.

Planavsky, N., Bekker, A., Rouxel, O.J., Kamber, B., Hofmann, A., Knudsen, A. and Lyons, T.W. (2010a) Rare Earth Element and yttrium compositions of Archean and Paleoproterozoic Fe formations revisited: New perspectives on the significance and mechanisms of deposition. *Geochimica et Cosmochimica Acta*, **74**, 6387–6405.

Planavsky, N.J., Rouxel, O.J., Bekker, A., Lalonde, S.V., Konhauser, K.O., Reinhard, C.T. and Lyons, T.W. (2010b) The evolution of the marine phosphate reservoir. *Nature*, **467**, 1088–1090.

Planavsky, N.J., Asael, D., Hofmann, A., Reinhard, C.T., Lalonde, S.V., Knudsen, A., Wang, X., Ossa, F.O., Pecoits, E., Smith, A.J.B., Beukes, N.J., Bekker, A., Johnson, T.M., Konhauser, K.O., Lyons, T.W. and Rouxel, O.J. (2014) Evidence for oxygenic photosynthesis half a billion years before the Great Oxidation Event. *Nature Geoscience*, **7**, 283–286.

Pokrovsky, O.S., Viers J. and Freydier, R. (2005) Zinc stable isotope fractionation during its adsorption on oxides and hydroxides. *Journal of Colloid and Interface Science*, **291**, 192–200.

Pokrovsky, O.S., Viers, J., Emnova, E.E., Kompantseva, E.I. and Freydier, R. (2008) Copper isotope fractionation during its interaction with soil and aquatic microorganisms and metal oxy(hydr)oxides: Possible structural control. *Geochimica et Cosmochimica Acta*, **72**, 1742–1757.

Poulton, S. and Canfield, D. (2005) Development of a sequential extraction procedure for iron: implications for iron partitioning in continentally derived particulates. *Chemical Geology*, **214**, 209–221.

Poulton, S.W. and Canfield, D.E. (2006) Co-diagenesis of iron and phosphorus in hydrothermal sediments from the southern East Pacific Rise: Implications for the evaluation of paleoseawater phosphate concentrations. *Geochimica et Cosmochimica Acta*, **70**, 5883–5898.

Poulton, S.W. and Raiswell, R. (2002) The low-temperature geochemical cycle of iron: From continental fluxes to marine sediment deposition. *American Journal of Science*, **302**, 774–805.

Raiswell, R. and Canfield, D.E. (1998) Sources of iron for pyrite formation in marine sediments. *American Journal of Science*, **298**, 219–245.

Raiswell, R. and Canfield, D.E. (2012) The Fe biogeochemical cycle past and present. *Geochemical Perspec*tives, **1**, 1−220.

Raiswell, R., Benning, L.G., Tranter, M. and Tulaczyk, S. (2008) Bioavailable iron in the Southern Ocean: the significance of the iceberg conveyor belt. *Geochemical Transactions*, **9**, 7.

Reinhard, C.T., Raiswell, R., Scott, C., Anbar, A.D. and Lyons, T.W. (2009) A late Archean sulfidic sea stimulated by early oxidative weathering of the continents. *Science*, **326**, 713−716.

Reinhard, C.T., Planavsky, N.J., Robbins, L.J., Partin, C.A., Gill, B.C., Lalonde, S.V., Bekker, A., Konhauser, K.O. and Lyons, T.W. (2013) Proterozoic ocean redox and biogeochemical stasis. *Proceedings of the National Academy of Science*, **110**, 5357−5362.

Richardson, L.L., Aguilar, C. and Nealson, K.H. (1988) Manganese oxidation in pH and O_2 microenvironments produced by phytoplankton. *Limnology and Oceanography*, **33**, 352−363.

Rickard, D. and Luther, G.W. III. (2007) Chemistry of iron sulfides. *Chemical Reviews*, **107**, 514−562.

Robbins, L.J., Lalonde, S.V., Saito, M.A., Planavsky, N.J., Mloszewska, A.M., Pecoits, E., Scott, C., Dupont, C.L., Kappler, A. and Konhauser, K.O. (2013) Authigenic iron oxide proxies for marine zinc over geological time and implications for eukaryotic metallome evolution. *Geobiology*, **11**, 295−306.

Robbins, L.J., Swanner, E.D., Lalonde, S.V., Eickhoff, M., Paranich, M.L., Reinhard, C.T., Peacock, C.L., Kappler, A. and Konhauser, K.O. (2015) Limited Zn and Ni mobility during simulated iron formation diagenesis. *Chemical Geology*, **402**, 30−39.

Roden, E.E. (2003) Fe(III) Oxide reactivity toward biological versus chemical reduction. *Environmental Science & Technology*, **37**, 1319−1324.

Roe, J.E., Anbar, A.D. and Barling, J. (2003) Nonbiological fractionation of Fe isotopes: evidence of an equilibrium isotope effect. *Chemical Geology*, **195**, 69−85.

Rouxel, O., Bekker, A. and Edwards, K. (2005) Iron Isotope Constraints on the Archean and Paleoproterozoic Ocean Redox State. *Science*, **307**, 1088−1091.

Ruttenberg, K. and Berner, R. (1993) Authigenic apatite formation and burial in sediments from non-upwelling, continental margin environments. *Geochimica et Cosmochimica Acta*, **57**, 991−1007.

Saito, M.A. and Moffett, J.W. (2001) Complexation of cobalt by natural organic ligands in the Sargasso Sea as determined by a new high-sensitivity electrochemical cobalt speciation method suitable for open ocean work. *Marine Chemistry*, **75**, 49−68.

Saito, M.A., Sigman, D.M. and Morel, F. M.M. (2003) The bioinorganic chemistry of the ancient ocean: the co-evolution of cyanobacterial metal requirements and biogeochemical cycles at the Archean-Proterozoic boundary? *Inorganica Chimica Acta*, **356**, 308−318.

Saito, M.A., Rocap, G. and Moffett, J.W. (2005) Production of cobalt binding ligands in a Synechococcus feature at the Costa Rica upwelling dome. *Limnology and Oceanography*, **50**, 279−290.

Sass, B.M. and Rai, D. (1987) Solubility of amorphous chromium(III)-iron(III) hydroxide solid solutions. *Inorganic Chemistry*, **26**, 2228−2232.

Satkowski, A.M., Beukes, N.J., Li, W., Beard, B.L. and Johnson, C.M. (2015) A redox-stratified ocean 3.2 billion years ago. *Earth and Planetary Science Letters*, **430**, 43−53.

Schauble, E.A. (2004) Applying stable isotope fractionation theory to new systems. Pp 65−111 in: *Geochemistry of Non-Traditional Stable Isotopes* (C.M. Johnson, B.L. Beard and F. Albarede, editors). Reviews in Mineralogy and Geochemistry, **55**. Mineralogical Society of America and the Geochemical Society, Washington, D.C.

Schauble, E.A. (2007) Role of nuclear volume in driving equilibrium stable isotope fractionation of mercury, thallium, and other very heavy elements. *Geochimica et Cosmochimica Acta*, **71**, 2170−2189.

Schauble, E., Rossman, G.R. and Taylor, H.P., Jr. (2004) Theoretical estimates of equilibrium chromium-isotope fractionations. *Chemical Geology*, **205**, 99−114.

Scott, C., Lyons, T.W., Bekker, A., Shen, Y., Poulton, S.W., Chu, X. and Anbar, A.D. (2008) Tracing the stepwise oxygenation of the Proterozoic ocean. *Nature*, **452**, 456−459.

Scott, C., Planavsky, N.J., Dupont, C.L., Kendall, B., Gill, B.C., Robbins, L.J., Husband, K.F., Arnold, G.L., Wing, B.A., Poulton, S.W., Bekker, A., Anbar, A.D., Konhauser, K.O. and Lyons, T.W. (2012) Bioavailability of zinc in marine systems through time. *Nature Geoscience*, **6**, 125−128.

Sherman, D.M. and Peacock, C.L. (2010) Surface complexation of Cu on birnessite (δ-MnO_2): controls on Cu in

the deep ocean. *Geochimica et Cosmochimica Acta*, **74**, 6721–6730.
Siebert, C., Nägler, T.F., von Blanckenburg, F. and Kramers, J.D. (2003) Molybdenum isotope records as a potential new proxy for paleoceanography. *Earth and Planetary Science Letters*, **211**, 159–171.
Siever, R. (1992) The silica cycle in the Precambrian. *Geochimica et Cosmochimica Acta*, **56**, 3265–3272.
Sikora, E.R., Johnson, T.M. and Bullen, T.D. (2008) Microbial mass-dependent fractionation of chromium isotopes. *Geochimica et Cosmochimica Acta*, **72**, 3631–3641.
Slack, J.F., Grenne, T., Bekker, A., Rouxel, O.J. and Lindberg, P.A. (2007) Suboxic deep seawater in the late Paleoproterozoic: Evidence from hematitic chert and iron formation related to seafloor-hydrothermal sulfide deposits, central Arizona, USA. *Earth and Planetary Science Letters*, **255**, 243–256.
Sreenivas, B. and Murakami, T. (2005) Emerging views on the evolution of atmospheric oxygen during the Precambrian. *Journal of Mineralogical and Petrological Science*, **100**, 184–201.
Staton, S.J.R., Amskold, L., Gordon, G., Anbar, A.D. and Konhauser, K.O. (2006) Iron isotope fractionation during photo-oxidation of aqueous ferrous iron. *Astrobiology*, **6**, 215–216.
Staubwasser, M., von Blanckenburg, F. and Schoenberg, R. (2006) Iron isotopes in the early marine diagenetic iron cycle. *Geology*, **34**, 629–632.
Stockdale, A., Davison, W., Zhang, H. and Hamilton-Taylor, J. (2010) The association of cobalt with iron and manganese (oxyhydr)oxides in marine sediment. *Aquatic Chemistry*, **16**, 575–585.
Stüeken, E.E., Catling, D.C. and Buick, R. (2012) Contributions to late Archaean sulphur cycling by life on land. *Nature Geoscience*, **5**, 722–725.
Sverjensky, D.A. (1984) Europium redox equilibria in aqueous solution. *Earth and Planetary Science Letters*, **67**, 70–78.
Sverjensky, D.A. and Sahai, N. (1996) Theoretical prediction of single-site surface-protonation equilibrium constants for oxides and silicates in water. *Geochimica et Cosmochimica Acta*, **60**, 3773–3797.
Swanner, E.D., Planavsky, N.J., Lalonde, S.V., Robbins, L.J., Bekker, A., Rouxel, O.J., Saito, M.A., Kappler, A., Mojzsis, S.J. and Konhauser, K.O. (2014) Cobalt and marine redox evolution. *Earth and Planetary Science Letters*, **390**, 253–263.
Tagliabue, A., Bopp, L., Dutay, J.-C., Bowie, A.R., Chever, F., Jean-Baptiste, P., Bucciarelli, E., Lannuzel, D., Remenyi, T., Sarthou, G., Aumont, O., Gehlen, M. and Jeandel, C. (2010) Hydrothermal contribution to the oceanic dissolved iron inventory. *Nature Geoscience*, **3**, 252–256.
Takahashi, Y., Manceau, A., Geoffroy, N., Marcus, M.A. and Usui, A. (2007) Chemical and structural control of the partitioning of Co, Ce, and Pb in marine ferromanganese oxides. *Geochimica et Cosmochimica Acta*, **71**, 984–1008.
Tessier, A., Fortin, D., Belzile, N., DeVitre, R.R. and Leppard, G.G. (1996) Metal sorption to diagenetic iron and manganese oxyhydroxides and associated organic matter: Narrowing the gap between field and laboratory measurements. *Geochimica et Cosmochimica Acta*, **60**, 387–404.
Thomazo, C., Nisbet, E.G., Grassineau, N.V., Peters, M. and Strauss, H. (2013) Multiple sulfur and carbon isotope composition of sediments from the Belingwe Greenstone Belt (Zimbabwe): A biogenic methane regulation on mass independent fractionation of sulfur during the Neoarchean? *Geochimica et Cosmochimica Acta*, **121**, 120–138.
Tossell, J.A. (2005) Calculating the partitioning of the isotopes of Mo between oxidic and sulfidic species in aqueous solution. *Geochimica et Cosmochimica Acta*, **69**, 2981–2993.
Tourtelot, H.A. (1979) Black shale – its deposition and diagenesis. *Clays and Clay Minerals*, **27**, 313–321.
Tréguer, P., Nelson, D.M., Van Bennekom, A.J., DeMaster, D.J., Leynaert, A. and Queguiner, B. (1995) The silica balance in the world ocean: a reestimate. *Science*, **268**, 375–379.
Trendall, A.F. and Blockley, J.G. (1970) The iron formations of the Precambrian Hamersley Group Western Australia with special reference to the associated crocidolite. *Geological Survey of Western Australia Bulletin*, **119**, 1–366.
Tribovillard, N., Algeo, T.J., Lyons, T. and Riboulleau, A. (2006) Trace elements as paleoredox and paleoproductivity proxies: An update. *Chemical Geology*, **232**, 12–32.
Twining, B.S. and Baines, S.B. (2013) The trace element composition of marine phytoplankton. *Annual Reviews in Marine Science*, **5**, 191–215.
Urey, H.C. (1947) The thermodynamic properties of isotopic substances. *Journal of the Chemical Society*,

562−580.

Urey, H.C. and Greiff, L.J. (1935) Isotopic exchange equilibria. *Journal of the American Chemical Society*, **57**, 321−327.

van Cappellen, P. and Wang, Y. (1996) Cycling of iron and manganese in surface sediments; a general theory for the coupled transport and reaction of carbon, oxygen, nitrogen, sulfur, iron, and manganese. *American Journal of Science*, **296**, 197−243.

Vine, J.D. and Tourtelot, E.B. (1970) Geochemistry of black shale deposits; a summary report. *Economic Geology*, **65**, 253−272.

Viollier, E., Jezequel, D., Michard, G., Pepe, M., Sarazin, G. and Alberic, P. (1995) Geochemical study of a crater lake (Pavin Lake, France) – Trace-element behaviour in the monimolimnion. *Chemical Geology*, **125**, 61−72.

Voegelin, A.R., Nägler, T.F., Samankassou, E. and Villa, I.M. (2009) Molybdenum isotopic composition of modern and Carboniferous carbonates. *Chemical Geology*, **265**, 488−498.

Voegelin, A.R., Nägler, T.F., Beukes, N.J. and Lacassie, J.P. (2010) Molybdenum isotopes in late Archean carbonate rocks: Implications for early Earth oxygenation. *Precambrian Research*, **182**, 70−82.

Wasylenki, L.E., Rolfe, B.A., Weeks, C.L., Spiro, T.G. and Anbar, A.D. (2008) Experimental investigation of the effects of temperature and ionic strength on Mo isotope fractionation during adsorption to manganese oxides. *Geochimica et Cosmochimica Acta*, **72**, 5997−6005.

Wasylenki, L.E., Weeks, C.L., Bargar, J.R., Spiro, T.G., Hein, J.R. and Anbar, A.D. (2011) The molecular mechanism of Mo isotope fractionation during adsorption to birnessite. *Geochimica et Cosmochimica Acta*, **75**, 5019−5031.

Wasylenki, L.E., Swihart, J.W. and Romaniello, S.J. (2014) Cadmium isotope fractionation during adsorption to Mn oxyhydroxide at low and high ionic strength. *Geochimica et Cosmochimica Acta*, **140**, 212−226.

Wasylenki, L.E., Howe, H.D., Spivak-Birndorf, L.J. and Bish, D.L. (2015) Ni isotope fractionation during sorption to ferrihydrite: Implications for Ni in banded iron formations. *Chemical Geology*, **400**, 56−64.

Weeks, C.L., Anbar, A.D., Wasylenki, L.E. and Spiro, T.G. (2007) Density functional theory analysis of molybdenum isotope fractionation. *Journal of Physical Chemistry, A*, **111**, 12434−12438.

Weeks, C.L., Anbar, A.D., Wasylenki, L.E. and Spiro, T.G. (2008) Density functional theory analysis of molybdenum isotope fractionation. *Journal of Physical Chemistry, A*, **112**, 10703−10704.

Welch, S.A., Beard, B.L., Johnson, C.M. and Braterman, P.S. (2003) Kinetic and equilibrium Fe isotope fractionation between aqueous Fe(II) and Fe(III). *Geochimica et Cosmochimica Acta*, **67**, 4231−4250.

Wen, H., Carignan, J., Cloquet, C., Zhu, X. and Zhang, Y. (2010) Isotopic delta values of molybdenum standard reference and prepared solutions measured by MC-ICP-MS: Proposition for delta zero and secondary references. *Journal of Analytical and Atomic Spectroscopy*, **25**, 716−721.

Wheat, C.G., Feely, R.A. and Mottl, M.J. (1996) Phosphate removal by oceanic hydrothermal processes: An update of the phosphorus budget in the oceans. *Geochimica et Cosmochimica Acta*, **60**, 3593−3608.

Widdel, F., Schnell, S., Heising, S., Ehrenreich, A., Assmus, B. and Schink, B. (1993) Ferrous iron oxidation by anoxygenic phototrophic bacteria. *Nature*, **362**, 834−836.

Wille, M., Kramers, J., Nägler, T., Beukes, N., Schröder, S., Meisel, T., Lacassie, J. and Voegelin, A. (2007) Evidence for a gradual rise of oxygen between 2.6 and 2.5 Ga from Mo isotopes and Re-PGE signatures in shales. *Geochimica et Cosmochimica Acta*, **71**, 2417−2435.

Williams, R. and Da Silva, J. (1996) The natural selection of the chemical elements. *Chemistry in Britain*. Clarendon Press, Oxford.

Wolthers, M., Charlet, L., van Der Linde, P.R., Rickard, D. and van Der Weijden, C.H. (2005) Surface chemistry of disordered mackinawite (FeS). *Geochimica et Cosmochimica Acta*, **69**, 3469−3481.

Wu, L., Percak-Dennett, E.M., Beard, B.L., Roden, E.E. and Johnson, C.M. (2012) Stable Fe isotope fractionation between aqueous Fe(II) and model Archean ocean Fe-Si coprecipitates and implications for Fe isotope variations in the ancient rock record. *Geochimica et Cosmochimica Acta*, **84**, 14−28.

Yamaguchi, K.E. (2002) *Geochemistry of Archean-Paleoproterozoic black shales: the early evolution of the atmosphere, oceans, and biosphere*. Ph.D. dissertation, Pennsylvania State University.

Zahnle, K., Claire, M. and Catling, D. (2006) The loss of mass-independent fractionation in sulfur due to a Palaeoproterozoic collapse of atmospheric methane. *Geobiology*, **4**, 271−283.

Zegeye, A., Bonneville, S., Benning, L.G., Sturm, A., Fowle, D.A., Jones, C., Canfield, D.E., Ruby, C., MacLean, L.C., Nomosatryo, S., Crowe, S.A. and Poulton, S.W. (2012) Green rust formation controls nutrient availability in a ferruginous water column. *Geology*, **40**, 599–602.

Zheng, Y., Anderson, R.F., van Geen, A. and Kuwabara, J. (2000) Authigenic molybdenum formation in marine sediments: a link to pore water sulfide in the Santa Barbara Basin. *Geochimica et Cosmochimica Acta*, **64**, 4165–4178.

Zink, S., Schoenberg, R. and Staubwasser, M. (2010) Isotopic fractionation and reaction kinetics between Cr(III) and Cr(VI) in aqueous media. *Geochimica et Cosmochimica Acta*, **74**, 5729–5745.